



Elisabeth Scheucher

**Synthesis and characterization of
multifunctional optical sensor particles for
a potential application in targeted drug
delivery**

DIPLOMARBEIT

zur Erlangung des akademischen Grades einer
Diplom-Ingenieurin
der Studienrichtung Allgemeine Technische Chemie
erreicht an der
Technischen Universität Graz

2010

Supervisors

Univ.-Prof. Dipl.-Chem. Dr.rer.nat. Ingo Klimant

and

Dipl.-Ing. Dr.techn. Günter Mistlberger

Institute of Analytical Chemistry and Food Chemistry
Graz University of Technology

Time flies like an arrow;
fruit flies like a banana

Danksagung

Es freut mich an dieser Stelle einigen Menschen danken zu dürfen. Ohne der Unterstützung vieler Personen wäre mein Weg bis zum Abschluss meines Studiums sehr viel schwieriger gewesen.

Ich möchte mich bei meinem Betreuer Univ.-Prof. Dipl.-Chem. Dr.rer.nat. Ingo Klimant bedanken, der es mir ermöglicht hat in seiner Arbeitsgruppe meine Diplomarbeit zu verfassen. Herzlichen Dank auch an meinen Mitbetreuer Dipl.-Ing. Dr.techn. Günter Mistlberger, der trotz meiner vielen Fragen (vor allem auch bezüglich der Verwendung von Computerprogrammen) nie die Nerven verloren hat und mir immer mit Rat und Tat zur Seite stand. Ohne seine hilfsbereite und freundschaftliche Unterstützung hätte die Arbeit sowohl im Labor als auch am Computer sicher viel weniger Spaß gemacht.

Neben meinen Betreuern möchte ich mich auch bei den Mitgliedern dieser Arbeitsgruppe bedanken, die für eine außergewöhnlich angenehme Atmosphäre verantwortlich sind. Immer ist jemand zur Verfügung um fachliche Diskussionen zu führen, Kaffee zu trinken oder einfach Spaß zu haben. Besonders bedanken möchte ich mich bei Daniel und Klaus für zahlreiche Gespräche und seelische Unterstützung als auch bei Sergey für sein unermessliches Fachwissen und seinen oft erheiternden konstruktiven Pessimismus. Vielen Dank an Birgit, Tobi, Gunter, Torsten, Babsi, Fabian und Clemens. Dank ihnen allen fällt es ein bisschen leichter in der Früh die wohlige Wärme des Bettes zu verlassen.

Für die tatkräftige Unterstützung bei der Erstellung der Diplomarbeit möchte ich mich bei meiner Schwester Eva bedanken, die für mich einige der künstlerisch wertvollen Zeichnungen gemacht hat. Danke auch an Christoph und Daniel für das Korrekturlesen und Daniel im Besonderen für die Versorgung mit warmen Speisen.

Zu guter Letzt will ich meiner Familie danken, die immer für mich da war. Ohne sie wäre ich wohl nicht in der Lage gewesen, so problem- und vor allem auch sorglos ein Studium abzuschließen.

Abstract

Optical sensors are established for a wide range of applications. Typically, they are planar foils or spots or they are attached to optical fibers. But due to their physical magnitude, they have some substantial drawbacks. For fiber optics, the measurements are always invasive. Foils and sensor spots have to be installed in a reaction vessel prior to measurement and are restricted to one spot. Sensor particles are able to overcome these drawbacks. The read out is noninvasive and no installation is necessary. The particles are simply added to the system to be analyzed and the resulting dispersion acts as the sensor.

For this thesis, magnetic optical sensor particles (MOSePs) were designed. Being magnetic, the particles can be separated by an external magnetic field. With a special set-up, collection of the particles in front of fiber optics is possible. This leads to higher signals and, consequently, a significantly smaller amount of particles needed for measurement compared to particle dispersions. Furthermore, the particles can be directed to any desired spot by moving the magnetic field.

The aim of this thesis was to design multifunctional MOSePs with a core-shell structure. By functionalization of the core and the shell, sensor particles for different applications could be realized. The synthesis of pH sensors, oxygen sensors with a temperature sensitive layer and fructose sensors was successfully carried out. With these particles targeted and noninvasive measurement of the analytes in aqueous medium is possible. Also application in microfluidics is feasible as the diameters of the MOSePs are below 200 nm. For further functionalization of the core-shell particles, also quantum dots were synthesized.

Kurzfassung

Optische Sensoren werden für eine Vielzahl von Anwendungen verwendet. Meist handelt es sich um Folien, Punkte oder an eine Faseroptik angebrachte Schichten. Allerdings besitzen sie aufgrund ihrer Größe einige Nachteile. Bei faseroptischen Sensoren ist nur eine invasive Messung möglich. Folien und Punkte müssen schon im Vorfeld im Reaktionsgefäß angebracht werden und sind auf die Messung an einem Punkt gebunden. Mit der Verwendung von Sensorpartikeln können diese Nachteile eliminiert werden. Das Auslesen der Messsignale ist ein nicht-invasiver Prozess und es sind auch keine vorbereitenden Schritte notwendig. Die Partikel werden einfach dem System zugegeben und als Dispersion ausgelesen.

In dieser Arbeit wurden magnetische optische Sensorpartikel (MOSePs) hergestellt. Durch ihre magnetischen Eigenschaften können diese durch ein extern angelegtes Magnetfeld gesammelt werden. Mit Hilfe von speziellen Magneten gelingt dies sogar direkt vor der Faseroptik. Dadurch kommt es zu stärkeren Signalen und es werden signifikant weniger Partikel für Messungen benötigt als dies bei Dispersionen der Fall ist. Zudem können die Partikel durch Verschiebung des Magnetfeldes zu jedem beliebigen Punkt gezogen werden.

Ziel dieser Arbeit war es, multifunktionelle MOSePs herzustellen. Durch eine Funktionalisierung des Kerns beziehungsweise der Hülle konnten Sensorpartikel für verschiedene Anwendungen synthetisiert werden. Die Herstellung von pH-Sensoren, Sauerstoffsensoren mit einer temperaturempfindlichen Hülle und Fruktosesensoren war erfolgreich. Unter Verwendung dieser Partikel kann eine ortsspezifische und nicht-invasive Messung der Analyten in wässrigen Medien durchgeführt werden. Da die MOSePs einen Durchmesser von weniger als 200 nm haben, ist auch eine Anwendung in mikrofluidischen Systemen möglich. Für eine weitere Funktionalisierung der MOSePs wurden auch Quantenpunkte hergestellt.

STATUTORY DECLARATION

I declare that I have authored this thesis independently, that I have not used other than the declared sources / resources, and that I have explicitly marked all material which has been quoted either literally or by content from the used sources.

Graz, May 31, 2010

Date

Signature

Abbreviations

Å	Ångström
AAM	acrylamide
ASRB	acryloylpiperaziny sulforhodamine B isomer
BA	boronic acid
BIS	<i>N,N'</i> -methylenebis(acrylamide)
DLS	dynamic light scattering
FLAC	<i>N</i> -fluorescein-acrylamide
fwhh	full width at half height
hPa	hectopascal
Ir(Cs) ₂ (acac)	Iridium (III) ((benzothiazol-2-yl)-7-(diethylamino)-cumarin) ₂ (acetylacetonat)
LED	light-emitting diode
mg	milligram
min	minute
mL	milliliter
mM	millimolar
mV	millivolt
MOSeP	magnetic optical sensor particle
nm	nanometer
ns	nanosecond
NIPAAm	<i>N</i> -isopropylacrylamide
PBS	phosphate buffered solution
PdTPTBPF	Palladium (II) meso-tetra(4-fluorophenyl)tetrabenzoporphyrin
pAAM	poly(acrylamide)
PMT	photomultiplier tube
pNIPAAm	poly(<i>N</i> -isopropylacrylamide)
PPS	potassium peroxydisulfate
PtTPTBPF	Platinum (II) meso-tetra(4-fluorophenyl)tetrabenzoporphyrin
QD	quantum dot
rpm	revolutions per minute
s	second
SDS	sodium dodecylsulfate
TOP	trioctylphosphine
TOPO	trioctylphosphine oxide
wt%	weight percent
μm	micrometer
μs	microsecond

Contents

I	Introduction	1
II	Theoretical background	5
1	Sensors	7
1.1	Classification	7
1.2	Chemical sensors	7
1.2.1	Optical sensors	8
1.2.2	Optical nanosensors	9
1.2.3	Magnetic optical sensor particles (MOSePs)	10
1.2.4	Core-shell particles	10
2	Photoluminescence	11
2.1	Absorption	11
2.2	Fluorescence	12
2.3	Fluorescence quenching	15
2.3.1	Förster resonance energy transfer (FRET)	16
2.4	Fluorescent pH dyes	17
2.4.1	Fluorescein	17
3	Magnetism	19
4	Quantum dots	21
4.1	Quantum confinement	21
4.2	Optical properties	21
4.3	Applications	22
5	Polymerization	23
5.1	Classification	23
5.2	Radical chain polymerization	24
5.3	Polymers	24
5.3.1	Hydrogels	24
5.3.2	Stimuli-responsive polymers	24
5.4	Immobilization of dyes in polymers	25
5.4.1	Drug delivery	25
6	Dynamic light scattering and zeta potential	27
6.1	Dynamic light scattering (DLS)	27

6.2	Zeta potential	27
III Experimental section		29
7	Materials	31
8	Core synthesis	33
8.1	Core precipitation	33
8.2	K _{SV} measurements	36
8.2.1	Ir(Cs) ₂ (acac)	36
8.2.2	PtTPTBPF and PdTPTBPF	36
9	Shell synthesis	37
10	Quantum dot synthesis	39
10.1	QD synthesis	39
10.2	Determination of the quantum yield	39
IV Results and discussion		41
11	Synthesis and characterization of core-particles	43
11.1	Influence of precipitation-parameters on the particle sizes	43
11.1.1	Polymer concentration	43
11.1.2	Direction of precipitation	44
11.1.3	Vortex speed	44
11.1.4	Flow rate of cocktail addition	44
11.1.5	Magnetite concentration	46
11.2	Functionalization of core particles	47
11.2.1	Ir(Cs) ₂ (acac)	47
11.2.2	PtTPTBPF	47
11.2.3	PdTPTBPF	48
12	Synthesis and characterization of quantum dots	51
12.1	Influence of the reaction time on the emission wavelength	51
12.2	Characterization of the produced QDs	51
12.3	Comparison of the synthesized quantum dots to commercially available QDs .	53
12.4	Incorporation of QDs in a sensor foil	54
12.5	Incorporation of QDs in particles	56
13	Polymerization and characterization of the shell	59
13.1	pNIPAAm - magnetic thermoresponsive oxygen sensors	59
13.2	Acrylamide - magnetic pH sensor particles	61
13.2.1	MOSePs for pH measurement	61
13.3	pNIPAAm - magnetic fructose sensor particles	64
13.3.1	Core-shell particles with a pNIPAAm/FLAC shell	65
13.3.2	Fructose/Glucose sensor particles	67

13.4 pNIPAAm - magnetic thermoresponsive particles for drug delivery?	70
13.4.1 Synthesis of the core-shell particles	70
13.4.2 Drug loading experiments	70
V Conclusions and outlook	73
14 Core particles	75
14.1 Precipitation	75
14.2 Functionalization	75
15 QDs	77
16 Core-shell particles	79
16.1 Oxygen sensors	79
16.2 pH sensors	79
16.3 Fructose sensors	79
16.4 Drug delivery	79
List of Figures	81
List of Tables	83
Bibliography	85

Part I

Introduction

Optical sensor particles provide a measurement system which is accessible for a wide range of applications. Those particles are very versatile. The sizes can be in the scale of nanometers up to millimeters, the composition ranges from coated metal spheres to hydrogel polymers, they can be beads, micelles or multi-layered particles, for example. Next to their structure and appearance, also a variety of analytes can be detected with optical sensor particles. Maybe the most important advantage of optical sensor particles is the fact that read-out is a noninvasive process.

The aim of this thesis was to produce core-shell particles, which can be upgraded by already known sensing systems. A very important functionalization all the beads had in common, was the incorporation of magnetite nanoparticles into the cores. The resulting spheres are referred to as Magnetic Optical Sensor Particles (MOSePs). Being magnetic, the particle can be directed by an external magnetic field to a desired spot. This minimizes the needed amount of particles for investigations, as the particles are not dispersed in the whole volume. By implementation of special separators the particles can be concentrated directly in front of fiber optics, thus leading to an enhanced signal.^{1,2} As the particles can be directed and read-out noninvasively, no preparation of the system to be analyzed has to be done. Furthermore, the particles can be used for imaging techniques in microfluidics, as their diameters are below 200 nm. With application of a magnetic field they are not washed away and can be kept in measuring position even though a flow is existing.

As already mentioned, the here presented MOSePs consist of a core-shell structure. The core particles are generated by a precipitation method, whereas the shell is added by radical chain polymerization. Two different hydrogels were used, one being known as a thermoresponsive polymer. Co-precipitation and co-polymerization of sensor dyes allow the further functionalization of the particles. By incorporation of sensor dyes it was possible to obtain oxygen sensors, pH sensors as well as fructose sensors. In every case it was verified that the sensing system can be applied to the core-shell particles.

Next to the functionalization with sensor dyes, also the application of the particles for targeted drug delivery was intended. However, the lack of experience in this area led to an underestimation of the complexity of such procedures. Unfortunately, no positive results can be presented in the field of drug delivery. However, also the experiments done for loading and release purposes brought a refinement in the employed polymerization technique. Polymerization of the shell was achieved emulsifier-free. The absence of this additive minimizes the necessary washing steps, thus yielding in a more economical production.

Part II

Theoretical background

1 Sensors

Since the aim of this diploma thesis was the design of novel multi functional optical sensor particles, this chapter is dedicated to sensors in general. The expression sensor originates from the Latin word “sentire” (to sense, to perceive). In principle, a sensor is a device which detects one or more properties and converts the information into a readable signal. Some of the most important characteristics of those devices are the fast response time, the direct contact with the system to be investigated, the ease of use and the transportability. Very often, a cheap production is also required.

1.1 Classification

Due to the multitude of existing sensors it became necessary to classify them. Some approaches organize them by grouping according to:

- the properties to be analyzed (e.g. physical or chemical sensors)
- the energy consumption (e.g. active or passive sensors)
- the transducer (e.g. optical or electrochemical sensors)
- the physical properties of the analytes (e.g. temperature sensor)
- the mode of application (e.g. in vivo / in vitro sensors)
- the duration of use (e.g. one-shot or continuous sensors).

Maybe the most popular differentiation is the one into physical and chemical sensors regarding the analyzed properties. For example, physical sensors are measuring the position, the shape, the distance, the acceleration, the mass or the temperature of a system, whereas chemical sensors observe the chemical composition.

1.2 Chemical sensors

The International Union of Pure and Applied Chemistry (IUPAC) describes a chemical sensor as “... a device that transforms chemical information, ranging from the concentration of a specific sample component to total composition analysis, into an analytically useful signal. The chemical information, mentioned above, may originate from a chemical reaction of the analyte or from a physical property of the system investigated.”³ Amongst others, this definition is based on the review of Janata and Bezegh.⁴ They claim that a sensor consists of a physical transducer and a chemically sensitive layer (figure 1.1). The receptor interacts specifically with an analyte and transforms the gained information, so it can be measured by the transducer. The latter converts and amplifies it into a readable output signal. Another extension to these definitions is the one of Wolfbeis, who adds the reversibility of the device.⁵

There are only a few exceptions of non-reversible sensor devices (e.g. the glucose sensor for diabetics). Again, there is a great variety of chemical sensors. That is why IUPAC decided to classify them according to the operating principle of the transducer.³ They suggest a division of chemical sensors into the following groups:

- optical devices
- electrochemical devices
- electrical devices
- mass sensitive devices
- magnetic devices
- thermometric devices
- others (for example x-ray or gamma-radiation)

Even though every one of them provides interesting information, I will take a closer look only on one of them - the optical devices.

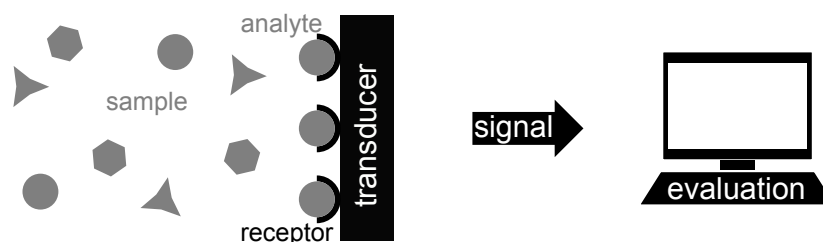


Figure 1.1: Set up of a typical sensor. The receptor interacts with the analyte and produces a signal which can be read out and amplified by the transducer.

1.2.1 Optical sensors

According to the definition mentioned above, optical sensors are working with the change of optical properties caused by the presence of the analyte. Possible interactions of electromagnetic waves with matter are:

- reflexion
- refraction
- absorption
- scattering including fluorescence and phosphorescence.⁶

All of those possibilities are being used in sensor technologies. There are two different working principles, depending on the optical properties. The first one is an intrinsic sensor where the analyte itself possesses detectable characteristics. In that case the receptor only needs to accumulate the analyte due to specific interaction in order to amplify the signal, for example. If the system to be investigated has no accessible optical properties, an extrinsic sensor is

needed. Here the receptor has to provide a signal which changes in the presence of the analyte. An example for extrinsic optical sensors based on fluorescence are oxygen sensors. In that case, a fluorescent dye is used as receptor and the luminescence, or more precisely, the phase of the emitted light is registered by a phase fluorimeter. If oxygen is present, the fluorescence of the dye is quenched. As a result, the emission light experiences a phase shift correlated to the oxygen concentration. Most optical sensors are using fiber optics or planar waveguide systems. Here, a significant advantage is the fact that fiber optics, developed and continuously ameliorated for communication systems, can be used unmodified. In figure 1.2 a typical setup for a fiber optic chemical sensor is shown.

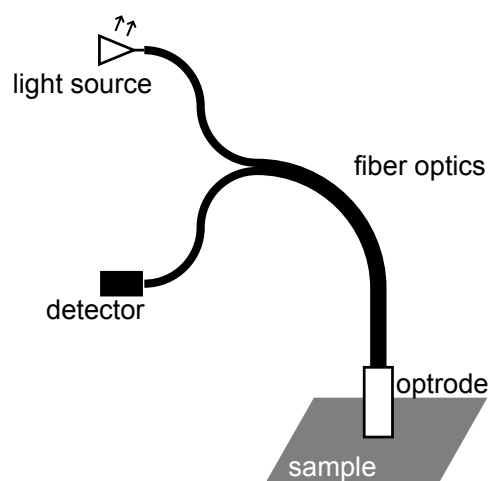


Figure 1.2: Components of an optical sensor. The light source, fiber optics, an optrode and a detector are shown.

1.2.2 Optical nanosensors

Typically, optical sensors are planar foils and spots, fiber optical sensors or micro sensors. Even though they are extremely versatile devices, they still are restricted in their application fields. The response time of foils and spots is quite long due to the required film-thickness. Their application area always has to be a surface on which they have to be fixed before measurement. Also, they are not suitable for microscopy or microfluidics.⁷ In order to overcome those drawbacks, optical nanosensors have been designed. Aylott describes them as "... devices that transduce a chemical or biological event using an optical signal, having all dimensions less than 1000 nm."⁸ One of the first introduced nanosensors are PEBBLEs (**p**robe **e**ncapsulated **b**y **b**io logically **l**ocalised **e**mbedding).⁹ Kopelman and coworkers designed particles in the range of 20 to 200 nm in diameter. Hydrophilic indicator dyes are entrapped in the pores of a hydrogel. As the dyes are protected by the polymer matrix, leakage is prevented. Also, a chemically and physically controlled micro environment is granted for measurements. PEBBLEs can be injected into living cells without harming them. In this way, determination of important cell parameters such as pH, oxygen- and calcium- concentration is possible.

1.2.3 Magnetic optical sensor particles (MOSePs)

The application of optical nanosensors in fluid systems has the disadvantage of needing high concentrations of particles in order to receive significant signals. A possibility to overcome that difficulty is the incorporation of magnetic particles into the sensors. Mistlberger et al. introduced such particles as well as an optimized magnetic separator for fiber optic applications.^{1,2,10} The MOSePs, which are dispersed in the system to be observed, can be separated in front of an optical fiber within minutes. For that reason, a significant smaller amount of sensor particles is needed, compared to non-magnetic systems. Also, the response time is much lower compared to similar setups with sensor foils or spots. By changing the location of the magnetic separator the particles will follow immediately and measurement of other regions is accessible.

1.2.4 Core-shell particles

Core-shell particles provide the possibility to obtain tailor-made properties. Those particles possess a spherical core which is surrounded by a layer of a different material. In this way, the characteristics of two substances can be combined in order to achieve a desired effect. As a result of their versatility they arouse interest in a variety of research areas. They may be used as semiconductors or magnetic composites, for catalysis, drug delivery, enzyme immobilization, molecular recognition, chemical sensing and many more.^{11–17} In case of using core-shell particles as MOSePs, it is very convenient to incorporate the magnetic components into the core and the fluorescent indicators into the shell. As a matter of fact, magnetite absorbs a considerable amount of light which is unfavorable for optical measurements. However, with this spatial separation the shell material can act as a shield to minimize absorption of the magnetite. Like this, direct placement of the core-shell particles by an external magnetic field is possible, without diminishing the fluorescence properties of the indicator dye significantly. As a shell material, stimuli responsive polymers can be introduced. A prominent example is poly(*N*-Isopropyl-acrylamide) (pNIPAAm), which reacts to a change of temperature by a drastic volume change (see section 5.3 on page 24). This behavior can be used for an application in drug delivery. Thereby, an active pharmaceutical ingredient is loaded onto the shell material. In case a magnetic core is used, precise drug targeting can be achieved by placing the particle by an external magnetic field and by changing the temperature. Because of that, pNIPAAm will undergo a phase transition, which results in the unloading of the agent.^{18–20} Another convenient utilization of the core-shell composition is the inclusion of toxic materials into the core. Like that, quantum dots could be used as donors in FRET systems for medical applications, for example.

2 Photoluminescence

If not indicated otherwise, the information of this chapter is based on the book “Molecular Fluorescence” by Valeur.²¹

The emission of light is generally called luminescence. The word originates from the Latin word “lumen”, which means “light”. In contrast to incandescence, luminescence is also called “cold light”. If the absorption of light (i.e. photons) leads to luminescence, it is called “photoluminescence”. When a molecule gets excited, it tends to lose this additional energy in order to return to an energetically stable condition. But emitting light is not the only way to do so. In figure 2.1 other possibilities are shown. As the behavior of a luminophor is extremely dependent on its microenvironment, fluorescence is well established for analytical analysis. If the analyte itself is fluorescent, direct fluorimetric detection is possible. Otherwise, some indirect methods are applicable. Some of them are the reaction of the analyte with a reagent yielding a fluorophor, formation of a fluorescent complex and fluorescence quenching. Latter is used to detect gases, such as oxygen, chlorine and sulfur dioxide.

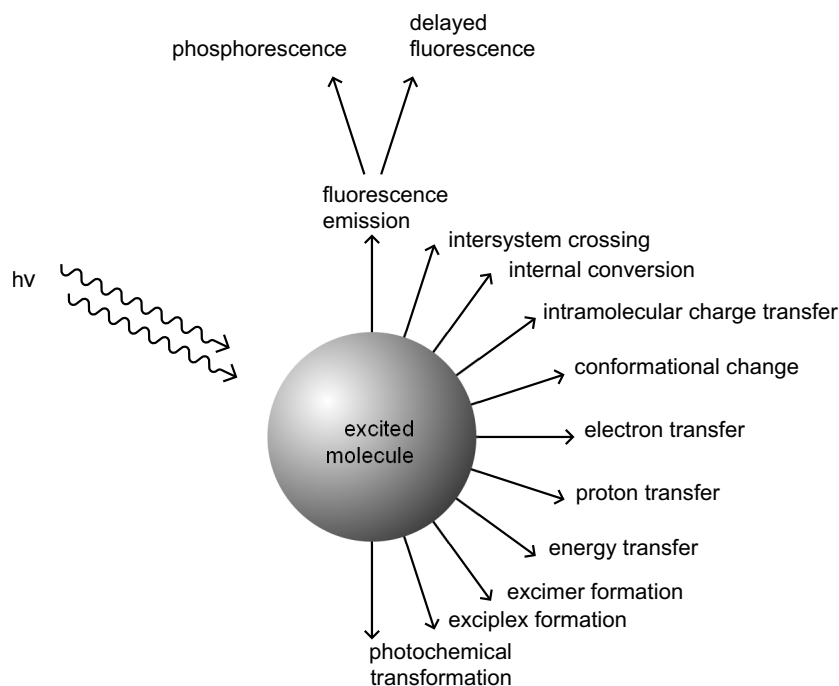


Figure 2.1: Possible relaxation pathways of an excited molecule.

2.1 Absorption

Absorption of photons can lead to a promotion of an electron from an orbital of the ground state to an unoccupied orbital of higher energies. In case of visible light, this means that

electrons from π bindings are affected. If light of much higher energy is used, such as one of the far UV, also σ bondings can be involved. According to the Pauli exclusion principle, two electrons which are located in the same orbital have to be of opposite spin. When an electron is promoted to a higher orbital, it usually maintains its spin. As the multiplicity of both states is equal to one, they are called singlet states. The multiplicity is calculated with equation 2.1, where M is the multiplicity and S the angular spin momentum.

$$M = 2S + 1 \quad (2.1)$$

If, for some later discussed reason, one electron changes its spin, the multiplicity will become three. Such a state is called triplet state, as there are three energetically equal states. According to Hund's rule, the singlet state possesses a higher energy than the triplet state of the same configuration. The abbreviations for the singlet ground state and the singlet and triplet excited states are S_0 , S_1 and T_1 . The energy which is absorbed is characteristic for a molecule because the energetic difference of excited and ground state is dependent on the molecule's composition. Also, every absorbing compound possesses a specific molar absorption coefficient (ϵ), which makes a quantitative measurement possible. Therefore, a photometer is used which is able to emit monochromatic light from VIS to UV, for example. After the light passes a cuvette containing the dissolved sample, the remaining intensity of light is measured. By correcting that information by the absorption of the used solvent, one can calculate the concentration of the analyte. The Beer-Lambert law (equation 2.2) is the base for this calculation.

$$E_\lambda = -lg(I/I_0) = \epsilon_\lambda * c * d \quad (2.2)$$

E_λ is the extinction at a certain wavelength, I_0 and I the intensity of the incident and passing light, c is the concentration of the sample and d the thickness of the cuvette.

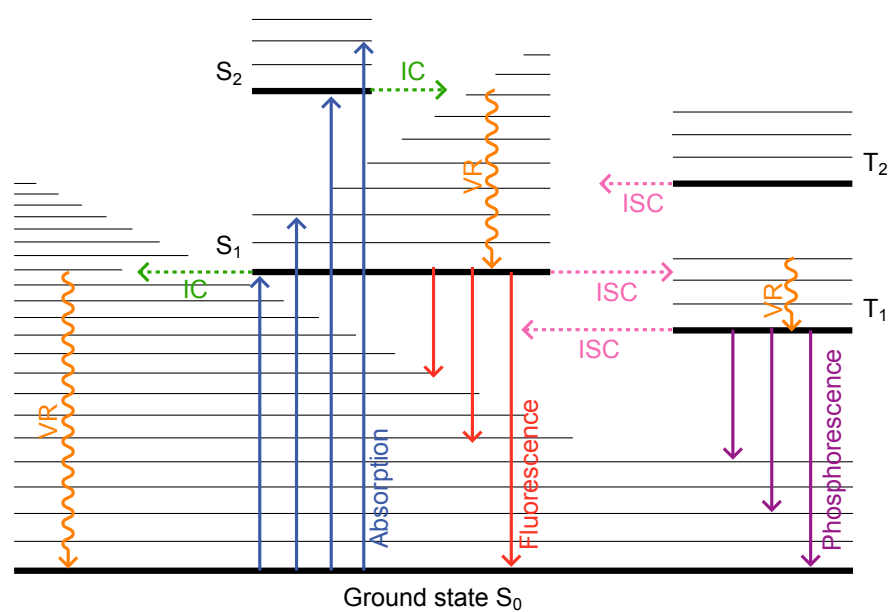
2.2 Fluorescence

Once a molecule is in its excited state different relaxation processes are possible, which are shown in the Perrin-Jablonski diagram (figure 2.2). Absorption starts from the lowest vibrational energy level of S_0 , because it can be assumed that nearly every molecule is in this state at room temperature. After excitation, the energy of the molecule can be on the first, second or higher singlet excited state. It does not have to be in the vibrational ground state of that energy level. By vibrational relaxation, it releases energy to solvent molecules until it is on the vibrational ground state. As this is the fastest process, it will always occur first. After that, other non-radiative or radiative transitions can occur.

Internal conversion (IC) is a transition between two electronic states of the same multiplicity where no light is emitted. It occurs within 10^{-13} - 10^{-11} seconds, when the molecule was excited to S_2 . Again, the first proceeding process is vibrational relaxation to the vibrational ground state of S_1 . Now again internal conversion to S_0 is possible, but highly unlikely as this energy gap is much higher than the one between S_2 and S_1 .

Fluorescence is one of the competing processes to internal conversion. The energy is released by emission of photons. Normally, fluorescence occurs from S_1 . For this reason, it is independent of the excitation wavelength. Here again, energy will be unleashed by vibrational

Perrin- Jablonski diagram



Legend

-  Internal Conversion, $S_i \rightarrow S_j$ non radiative transition.
-  InterSystem Crossing, $S_i \rightarrow T_j$ non radiative transition.
-  Vibrational Relaxation.

Figure 2.2: The Perrin-Jablonski diagram presents different possibilities of relaxation.

relaxation. The gap between the maximum of absorption and fluorescence is called Stoke's shift. The origin of this gap is obvious. Some of the energy which excited the molecule was released by vibrations. For fluorescence only a part of this energy is accessible.

Intersystem crossing (ISC) is the other process, next to fluorescence, which competes internal conversion. This transition is a non-radiative one towards T_1 , including a change of the spin. In principle, this process is forbidden, but spin-orbit coupling, especially in presence of heavy atoms, can facilitate it.

Phosphorescence is the radiative transition between T_1 and S_0 . As this transition is also forbidden, only spin-orbit coupling can render it possible. However, due to the long lifetime of this excited state, the probability of a non-radiative relaxation, particularly in solution, is very high.

Delayed fluorescence is possible, when another intersystem crossing (T_1 to S_1) occurs. The emission wavelength is the same as with normal fluorescence, but the decay time is much longer. Table 2.1 quotes the characteristic times for the processes mentioned above.

Table 2.1: Characteristic decay times of photophysical processes.

Process	Decay time (s)
absorption	10^{-15}
vibrational relaxation	10^{-12} - 10^{-10}
fluorescence	10^{-10} - 10^{-7}
intersystem crossing	10^{-10} - 10^{-8}
internal conversion	10^{-11} - 10^{-9}
phosphorescence	10^{-6} -1
delayed fluorescence	10^{-6} -1

The life times of excited states can be calculated by considering the rate constants for the various processes. For example, the lifetime of the excited state S_1 can be derived from equation 2.3. Here, τ_S is the lifetime of S_1 and k_r^S and k_{nr}^S the rate constants for radiative respectively non-radiative deactivation.

$$\tau_S = \frac{1}{k_r^S + k_{nr}^S} \quad (2.3)$$

Another important characteristic is the fluorescence quantum yield (Φ_F). It indicates the fraction of molecules which return to ground state S_0 under emission of light (equation 2.4).

$$\Phi_F = \frac{k_r^S}{(k_r^S + k_{nr}^S)} = k_r^S \tau_S \quad (2.4)$$

2.3 Fluorescence quenching

Next to the intrinsic processes mentioned above there are also intermolecular photophysical processes. The most important are:

- collision with a heavy atom or a paramagnetic species
- electron transfer
- excimer formation
- exciplex formation
- proton transfer
- energy transfer

Each of these processes leads to quenching (i.e. loss of fluorescence energy) of the primarily excited molecule. One of the most important quenchers is oxygen, as it is omnipresent. Oxygen is a paramagnetic substance. That means, its ground state is a triplet state ($^3\text{O}_2$). It possesses two low energetic, but still unstable, singlet states ($^1\Delta$ and $^1\Sigma$). By collision of an excited molecule with triplet oxygen, the molecule loses its energy and oxygen becomes excited to one of its singlet states. Under atmospheric pressure and in air-saturated solutions, the life time of any fluorophore can not be longer than $10^{-6} - 10^{-7}$ seconds. The quenching of fluorescent molecules by oxygen follows the Stern-Volmer kinetics of dynamic quenching. At this approach, the quenching rate constant k_q is assumed to be time-independent. Equation 2.5 shows the *Stern-Volmer relation*:

$$\frac{\Phi_0}{\Phi} = \frac{I_0}{I} = \frac{\tau_0}{\tau} = 1 + K_{SV}[Q] \quad (2.5)$$

K_{SV} , the Stern-Volmer constant is the product of k_q and τ_0 . In a Stern-Volmer plot, I_0/I is plotted against the quencher concentration $[Q]$. In case of a linear dependency, the slope equals K_{SV} .

The Stern-Volmer plot of immobilized fluorophores is very often not exactly linear. The slope is flattening at high oxygen concentrations. This is a well known phenomenon and originates from the location of the fluorophore molecules. Molecules located on or near the surface are accessible for oxygen and therefore are quenched. In contrast, molecules which are surrounded by the matrix can not or only slightly be quenched by oxygen. In case the Stern-Volmer plot leads to such a flattened curve the two-site model of Carraway et al.²² can be applied (2.6). Here, two fractions (f_1 and f_2) of fluorophore molecules are assumed. These fractions possess different quenching constants (K_{SV1} and K_{SV2}) as a result of their position in the matrix. As this is a very complex approach with many variables, the simplified two-site model of Klimant et al.²³ can be used instead. In this model one fraction (f_1) is assumed to be quenchable while the other one (f_2) is unquenchable ($K_{SV2} = 0$) (equation 2.7).

$$\frac{\tau_0}{\tau} = \left[\frac{f_1}{1 + K_{SV1}[Q]} + \frac{f_2}{1 + K_{SV2}[Q]} \right]^{-1} \quad (2.6)$$

$$\frac{\tau_0}{\tau} = \left[\frac{f_1}{1 + K_{SV1}[Q]} + f_2 \right]^{-1} \quad (2.7)$$

To obtain the values of I , I_0 , τ and τ_0 for the calculation of K_{SV} , a phase-modulated fluorimetric experiment has to be done. Here, a sinusoidally modulated light with a high frequency is used for sample excitation. The fluorophor possesses a characteristic lifetime and phase in absence of oxygen (τ_0 and ϕ_0). By quenching, these values are altered. Equations 2.8 and 2.9 provide the basis for calculation.

$$\tau = \frac{\tan\Phi}{2\pi f} \quad (2.8)$$

$$I = \frac{A}{M} = A * \sqrt{1 + (\tau 2\pi f)^2} \quad (2.9)$$

Here, f is the frequency of the modulation, A the amplitude of the measured signal and M the demodulation.

2.3.1 Förster resonance energy transfer (FRET)

As the Förster resonance energy transfer plays an important role in many optical sensor applications, as well as in some experiments of this diploma thesis, a short introduction to the fundamentals is necessary. In general, resonance energy transfer (RET) is a non-radiative transfer of excitation energy from a donor molecule to an acceptor molecule. A spectral overlap of the absorption spectrum of the acceptor and the emission spectrum of the donor is required. Some of these transition states have the same energy, which means that they are in resonance. There are different interactions possible, leading to energy transfer. Förster's mechanism describes long-range dipole-dipole Coulombic interactions. Other possibilities are multipolar Coulombic interactions and intermolecular orbital overlap, including electron exchange (Dexter mechanism) and charge resonance interactions. Förster stated that the rate constant for energy transfer (k_T) of a donor and an acceptor at the distance r is dependent on the excited-state lifetime of the donor (τ_D^0) and the Förster critical radius (R_0):

$$k_T = \frac{1}{\tau_D^0} \left\{ \frac{R_0}{r} \right\}^6 \quad (2.10)$$

R_0 describes the distance between donor and acceptor, where energy transfer and spontaneous decay of the excited donor are equally probable. Equation 2.11 describes the calculation of this term (R_0 in Å).

$$R_0 = 0.2108 \left\{ \kappa^2 \Phi_D^0 n^{-4} \int_0^\infty I_D(\lambda) \epsilon_A(\lambda) \lambda^4 d\lambda \right\}^{1/6} \quad (2.11)$$

κ^2 is an orientational factor (ranging from 0 to 4, respectively from perpendicular to collinear transition moments), Φ_D^0 is the fluorescence quantum yield of the donor when no transfer takes place, n is the average refractive index of the medium in the range of the spectral overlap, $I_D(\lambda)$ is the normalized fluorescence spectrum of the donor, $\epsilon_A(\lambda)$ is the molar extinction coefficient of the acceptor (in $\text{dm}^3 \text{mol}^{-1} \text{cm}^{-1}$) and λ is the wavelength in nanometers. Förster's critical radius is in the range of 10 to 80 Å. The transfer efficiency (Φ_T) is given by equation 2.12.

$$\Phi_T = \frac{k_T}{1/\tau_D^0 + k_T} = \frac{1}{1 + (r/R_0)^6} \quad (2.12)$$

The transfer efficiency is extremely sensitive to the distance between donor and acceptor, as the sixth power of the quotient of the distance to Förster's radius indicates.

2.4 Fluorescent pH dyes

Fluorescent indicators are extensively used in analytical chemistry, bioanalytical chemistry and medicine. They are employed for pH and pCO₂ measurements, for example in cells or blood. As they have a higher sensitivity than the classical pH dyes based on color change, such as phenolphthalein or thymol blue, they are highly desired. They can also be used in fluorescence microscopy and for fiber optic sensors. Basis for the determination of the pH by fluorescent indicators is the Henderson-Hasselbalch equation (2.13), where $[A]$ and $[B]$ are the concentrations of the acidic, respectively the basic form.

$$pH = pK_a + \log \frac{[B]}{[A]} \quad (2.13)$$

To adapt this equation for fluorometric titrations, the concentration is replaced by fluorescence intensity. I is the measured intensity and I_A and I_B are the intensities at the same wavelength when the indicator is only in its acidic or basic form (equation 2.14).

$$pH = pK_a + \log \frac{I - I_A}{I_B - I} \quad (2.14)$$

The Henderson-Hasselbalch equation is based on a simplification. It disregards that pH is a value of the activity of protons rather than the concentration of protons. As the activity is the product of the amount fraction and the activity coefficient (f), the pK_a is dependent not only on temperature, but also on factors having an influence on the activity coefficients. These are the ionic strength of the media, specific interactions depending on the chemical nature of the indicator and structural changes of the medium.

2.4.1 Fluorescein

Fluorescein is an indicator dye which is nearly independent of ionic strength. It is used in a variety of applications. Its pK_a values are 2.2, 4.4 and 6.7 (figure 2.3). As there are two subsequent transitions (neutral \rightarrow monoanion \rightarrow dianion) it possesses a broad range of pH response. By derivatization it is possible to change the pK_a . For example, BCECF (2',7'-bis(carboxyethyl)-5(or6)-carboxyfluorescein) has a pK_a near to 7, which makes it suitable for intracellular applications.

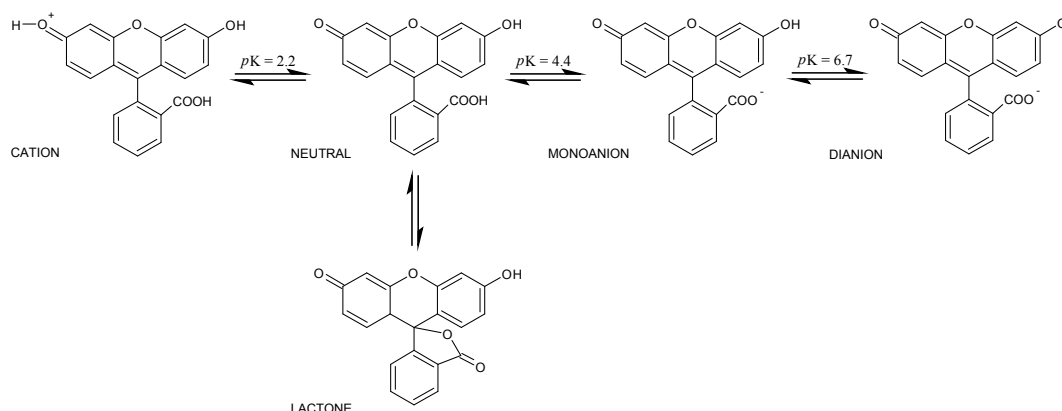


Figure 2.3: Forms of fluorescein in aqueous solution.

3 Magnetism

As the sensor particles developed during this diploma thesis are magnetic, a short introduction into magnetism is appropriate. This chapter is based on the book “Anorganische Chemie” by Riedel.²⁴ A magnetic field is described by magnetic induction or magnetic flux density (B in Tesla respectively in Vs/m²) or the magnetic field strength (H in A/m). The dependency is described in equation 3.1, where μ_0 is the magnetic field constant.

$$B = \mu_0 H \tag{3.1}$$

A body in a homogeneous magnetic field with the induction $B_{outside}$ exhibits a magnetic field of the new induction B_{inside} . The factor which describes this dependency is called relative permeability μ_r (equation 3.2).

$$B_{inside} = \mu_r B_{outside} \tag{3.2}$$

The magnetic capacitance is called susceptibility (χ_V). It can be derived from equations 3.3 and 3.4.

$$B_{inside} = B_{outside} + J \tag{3.3}$$

$$J = \chi_V B_{outside} \tag{3.4}$$

Here, J is the magnetic polarization.

Matter can be divided into three types of magnetism: diamagnetic matter, paramagnetic matter and ferromagnetic matter (table 3.1, figure 3.1). The flux density in diamagnetic materials is smaller than outside, whereas in para- and ferromagnetic matter it is bigger.

Table 3.1: The three types of magnetism and their values for relative permeability (μ_r) and susceptibility (χ_V).

Magnetism type	μ_r	χ_V
diamagnetism	< 1	< 0
paramagnetism	> 1	> 0
ferromagnetism	>> 1	>> 0

Diamagnetism. Materials whose electrons are paired do not have a magnetic moment, as the spin moments of the electrons compensate each other. Due to intermolecular bonds unpaired electrons become saturated. This is why most materials are diamagnetic. A magnetic field induces a magnetic polarization which is opposite to the outer field. As a result, the magnetic flux density inside the body is lower than outside. Also, the diamagnetic susceptibility is independent on field strength and temperature.

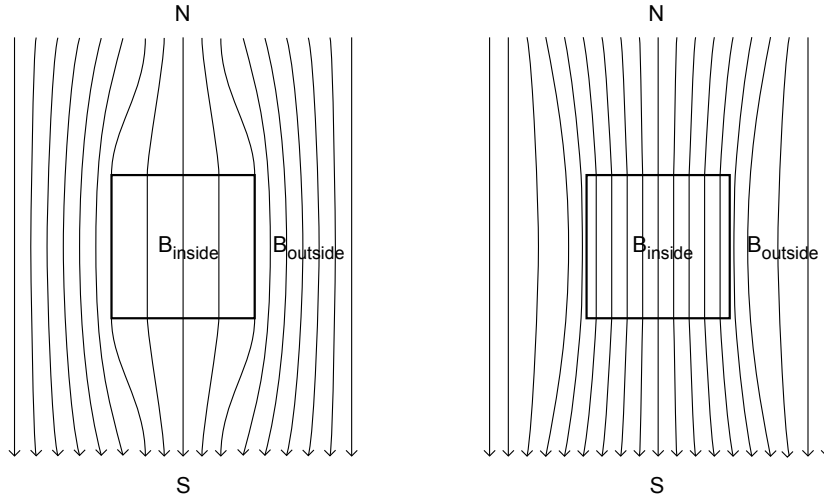


Figure 3.1: Diamagnetic and paramagnetic matter. In diamagnetic matter (left) the flux density inside the body is lower than outside. In paramagnetic matter (right) it is higher.

Paramagnetism. Materials with unpaired electrons show permanent magnetic moments which are statistically distributed and therefore cancel each other out. If an outer magnetic field is present, the magnetic moments align to it. A magnetic field with the same direction as the first one is generated. Paramagnetism is stronger than diamagnetism by several orders of magnitude. For such paramagnetic matter, the susceptibility is independent on field strength but dependent on temperature because a higher temperature is counteracting the orientation of the magnets. The temperature dependency is described by Curie's law (equation 3.5 and 3.6).

$$\chi_{para} = \frac{C}{T} \quad (3.5)$$

$$C = \frac{\mu_0 N_A}{3k} \mu_{mag}^2 \quad (3.6)$$

Here, C is the Curie constant, N_A the Avogadro constant, k the Boltzmann constant and μ_{mag} the magnetic moment.

Ferromagnetism. Only iron, nickel and cobalt are ferromagnetic at room temperature. Below the Curie temperature (T_C) all spins within magnetic domains, called Weiss domains, are aligned. The material is not magnetic, as those domains are counteracting. The susceptibility is highest when the temperature reaches absolute zero. When an external magnetic field is applied, magnetization occurs because all magnetic moments of the Weiss domains align to the outer field and the material becomes magnetic itself. When the external field is removed, a magnetic remanence is still existing as the magnetization follows a hysteresis curve. Above Curie temperature, the ferromagnetism breaks down and Curie's law is valid again.

4 Quantum dots

Quantum dots (QDs) are nanocrystallites with diameters in the range of 1 nm to 100 nm. They are semiconductors which possess very special properties. QDs mark the link between molecules and large crystals. They show discrete electronic transitions, such as atoms and molecules do. As they are semiconductors, they also possess a band gap energy (E_g). This amount of energy has to be applied in order to excite an electron from the valence band to the conduction band. A photon which gets absorbed can deliver this energy. In this way, a positively charged hole in the valence band and a negatively charged electron in the conduction band are generated. This electron-hole pair is called exciton. In the course of the relaxation process, where the exciton is destroyed by recombination, photons can be emitted.²⁵

4.1 Quantum confinement

Excitons have, depending on the crystal material, a finite size called the Bohr exciton diameter (a_B). Typically, it spans the region between 1 and 100 nm. If it happens that the dimension of the crystal is smaller than the Bohr exciton diameter of this material, a formed exciton becomes spatially confined. As a result, its energy is increasing. For that reason, the size of the exciton defines the region of quantum confinement regime. Crystals, which are smaller than the Bohr exciton diameter exhibit absorption and fluorescence which is dependent on the crystal size.²⁵

4.2 Optical properties

There are some significant advantages of quantum dots over conventional fluorescent dyes. First of all, the emission wavelength of quantum dots can easily be adjusted by the size of the crystals from blue to near infrared. Also, the emission peak is narrow with dimensions of approximately 20 to 40 nm full width at half maximum. Secondly, they absorb photons from the ultraviolet to the visible, due to their broad continuous absorption spectra. Even though they possess an absorption maximum at the wavelength corresponding to their band gap, known as the quantum-confinement peak, they also absorb at higher energies. This property can be used to excite multicolor quantum dots with just one wavelength of incident light. The slight disadvantage of lower quantum yields compared to organic dyes is outweighed by their larger absorption cross section as well as their distinct photostability.^{26,27} The shape of the nanocrystals has an impact on its optical properties, too. Quantum rods, for example, emit nearly polarized light and have a wide Stoke's shift.²⁸ Next to the shape, the surface of the particles plays an important role. The atoms of the surface are not saturated. This is why they have one or more "dangling orbitals" which project the surface. These unpassivated orbitals may form band structures located within the band gap of the nanocrystal. If that happens, they can trap charge carriers and reduce the overlap between electron and hole. That would lead to a higher probability of non-radiative decay. The dangling orbitals can be passivated

by embedding the nanocrystals into another crystal or glass, or by attachment of coordinative ligands such as trioctylphosphine oxide (TOPO). Furthermore, the nonpolar residues make the particles soluble in organic solvents.²⁵ By deposition of a ZnS layer by epitaxial growth around CdSe quantum dots, absorption undergoes a slight red-shift. Furthermore, the quantum yield is increased from 5-15 % of bare quantum dots to 15-30 % of passivated ones.²⁹

4.3 Applications

In the last ten years, a lot of research has been done in the field of quantum dots. Not only to advance their performance but also to integrate them into a variety of applications. Quantum dots are used as luminescent labels for biomedical imaging, as probes for sensors^{30,31} and biosensors,³² as materials for optoelectronic devices³³ and for quantum computing.³⁴ An application of high interest is the use of quantum dots as FRET donors.^{32,35,36} The usage of just one excitation wavelength for a simultaneous measurement of analytes is an interesting aspect. According to the absorption spectra of the used luminescent sensor dyes, quantum dots with such emission wavelengths can be synthesized. As they possess a broad continuous absorption spectrum, irradiation of a single wavelength of high energy is sufficient to excite every one of the sensor dyes. This setup minimizes interferences of the diverse excitation and emission wavelengths of the used dyes.

5 Polymerization

If not indicated otherwise, information of this chapter is provided by the book “Principles of Polymerization” by George Odian.³⁷

A short overview about polymerization and polymers used in this thesis is given in this chapter. According to IUPAC, a polymer is a “... molecule of high relative molecular mass, the structure of which essentially comprises the multiple repetition of units derived, actually or conceptually, from molecules of low relative molecular mass”.³⁸

5.1 Classification

Two kinds of classification exist. The first one is introduced by Carothers in 1929. It is based on the compositional difference of the polymer and the monomers it is built of. Condensation polymers are generated by reactions where small molecules, such as water, are eliminated. A famous representative of this group is poly(hexamethylene adipamide), also known as nylon 6/6. The repeating unit does not have the same composition as the monomers. On the contrary, addition polymers are built without elimination of small molecules. Here, repeating unit and monomer possess the same composition. Those monomers have to feature carbon-carbon double bonds. The characteristic moiety is called vinyl ($\text{CH}_2=\text{CH}-$). An example is poly(styrene). The other classification by Flory (1953) is based on the polymerization mechanism. Step polymerizations are characterized by a step by step reaction between the functional groups of the monomers. The polymers are growing relatively slow and every unit (monomer, dimer, trimer etc.) can react with each other. In chain polymerization, the situation is a completely different one. Here an initiator creates a reactive center. That can be a free radical, cation or anion. Monomers add consecutively in a chain reaction, propagating the reactive center (figure 5.1). Once a reactive center is destroyed by a termination reaction the polymerization ends.

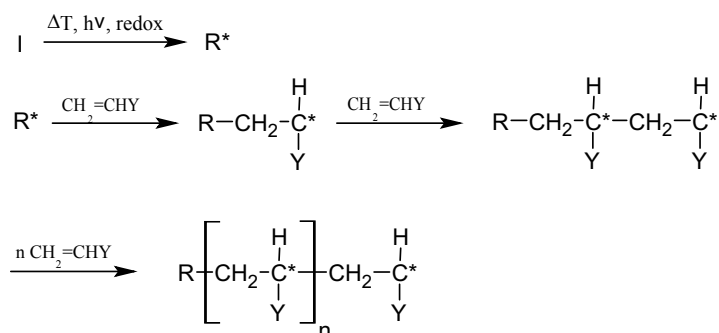


Figure 5.1: Chain polymerization scheme. (I = initiator, R^* = reactive species (radical, cation or anion))

5.2 Radical chain polymerization

A radical chain polymerization consists of three stages. At first, the initiator (I) is transformed into a free radical (R^*). This can happen by thermal decomposition, a redox reaction or a photochemical initiation. The generated radical undergoes a reaction with a monomer (M), yielding a initiator-monomer-complex (RM^*). Then, the chain propagation occurs, where monomers add to the complex and prolongate the radical polymer chain. The growth of the polymer is very fast compared to step polymerization. Chain propagation is ongoing until chain termination occurs. Two radicals can couple and form a single molecule. This is the most common reaction and is called recombination. Also, chain disproportionation is possible. Again, two radicals meet and exchange a proton, leaving two terminated chains. One is saturated and the other one has a terminal double bond (figure 5.2).

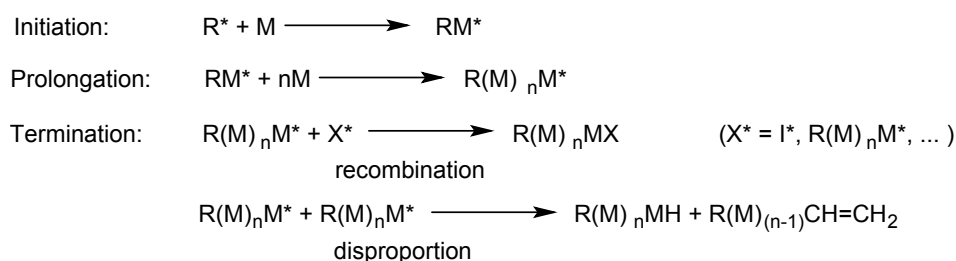


Figure 5.2: The three stages of a radical chain polymerization

5.3 Polymers

A multitude of different kinds of polymers is existing. For example, there are thermoplasts, which can be deformed in a hot state and harden when they cool down, or elastomers, which behave like rubber. Two special forms are hydrogels and stimuli-responsive polymers.

5.3.1 Hydrogels

Hydrogels are polymers which are able to swell in aqueous media. Due to cross-linking they are insoluble, but can contain more than 99 % water. They are highly biocompatible and low toxic, what makes them interesting for medical and biomedical utilization.³⁹ Hydrogels are also widely used for drug delivery applications.^{40,41} The most common hydrogels are based on chitosan, gelatin and other biopolymers. Others are acrylamide and polyacrylic acid.

5.3.2 Stimuli-responsive polymers

Stimuli-responsive polymers respond to changes in their environment with property changes. These polymers can be sensitive to temperature, pH, ionic strength, light, electric or magnetic fields. They can change in shape, surface characteristics, solubility or perform a sol-gel transition. These unique properties make them suitable for many medical applications, such as tissue engineering, drug-delivery and sensor technology.⁴²

pNIPAAm or poly(N -isopropylacrylamide) is a synthetic thermoresponsive polymer. Its lower critical solution temperature (LCST) in water is 32°C. Below this temperature it is

hydrated and swollen, above it becomes hydrophobic and collapses. It experiences a sharp coil-globule transition at the LCST. At temperatures below the LCST the hydrogen bonding between the polymer chains and water are predominant, thus they have a water-soluble coiled structure. On the other hand, above the LCST, hydrogen bondings between the carbonyl and N-H groups in the polymer chains lead to a compact structure which pushes out the water molecules. An interesting aspect about pNIPAAm is the possibility to control the LCST by incorporating charged units. In general, hydrophilic moieties increase the LCST, whereas hydrophobic residues lower the LCST. This makes it possible to shift the LCST to body temperature, making pNIPAAm an interesting polymer for applications such as drug delivery.^{18–20,43}

5.4 Immobilization of dyes in polymers

As mentioned before (chapter 1), molecules, such as fluorescent indicators, can be immobilized in a polymer. One possibility is to entrap them in cavities of the matrix. Interactions between dye and polymer, for example hydrophobic or hydrophilic ones, lead to a relatively weak bonding, holding the molecules captive. If these interactions are too weak or if possible interactions with the solvent are stronger, the dye will leach out. In order to avoid leaching, the dye can also be immobilized by covalent binding. Here, the polymer or the indicator molecule has to be modified to provide access to chemical linkage. One of the favored derivatizations is the addition of an acryl moiety to the indicator molecule. By this, functionalities can be introduced by co-polymerization of matrix and dye-molecules. Two modified fluorophores used in this thesis are *N*-fluoresceinacrylamide (FLAC) and acryloylpiperaziny sulforhodamine B (ASRB) (figure 5.3).

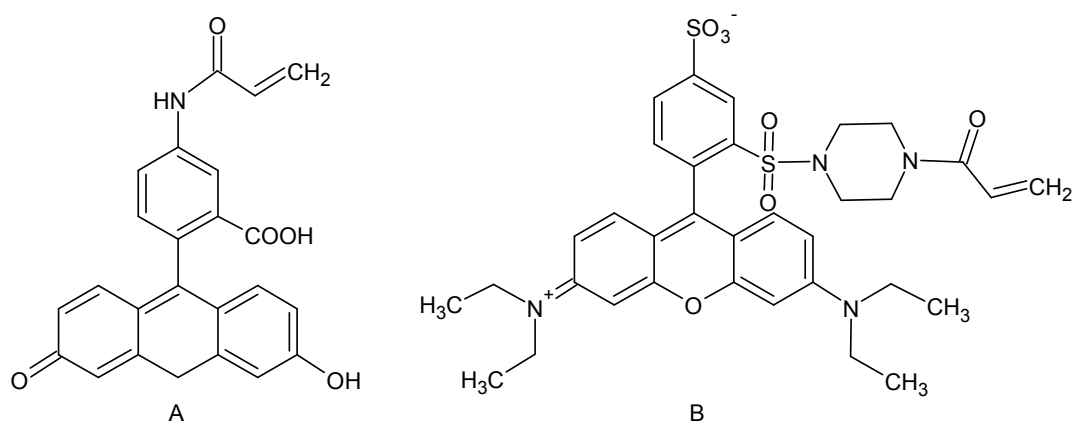


Figure 5.3: Structures of the used dyes, modified for co-polymerization. (A) *N*-fluoresceinacrylamide (FLAC) and (B) acryloylpiperaziny sulforhodamine B (ASRB).

5.4.1 Drug delivery

Immobilization of molecules by hydrophilic or hydrophobic interactions is widely used for drug delivery. Here, often a hydrogel is utilized as matrix. When loaded with an agent, it can release it in the desired tissue either because of diffusion or a change of a property of the environment.^{40,41} For the latter, stimuli responsive polymers are necessary. A popular

polymer for drug delivery is pNIPAAm, as it responds to temperature changes. This attribute is advantageous, as it is possible to heat specific regions of the body. Like this, pharmaceutical active ingredients can be released directly at the harmed tissue. By using MOSePs, an external magnetic field can direct the particles to the desired spot. By application of an alternating magnetic field heat is generated, also leading to detachment of the agent.²⁰ An advanced attempt is to use a mesoporous matrix, such as silica or dextran derivatives, which is surrounded by a pNIPAAm layer. Here, the drug is loaded into the mesoporous material while the temperature responsive polymer is acting as a gate. At temperatures below the LCST, trapped agents are withheld. Above the LCST the gates open and release is initiated.^{18,44}

6 Dynamic light scattering and zeta potential

The information of this chapter is based on the website of Malvern,⁴⁵ a provider of instruments for material characterization. Here, an overview about the principles of the following measurements is allocated.

6.1 Dynamic light scattering (DLS)

DLS is a noninvasive measurement of the hydrodynamic diameter of particles. Typically, size and size distribution of particle emulsions in the sub micron region are measured. The measurement is based on Brownian motion, the random movement of particles caused by collision with solvent molecules. The velocity of the Brownian motion is dependent on the size of the particles. The larger they are, the slower they move. Of course, also the viscosity of the solvent is a crucial parameter. For the measurement a constant temperature has to be provided, in order to exclude convection. According to the Stokes-Einstein equation (6.1), the hydrodynamic diameter ($d(H)$) is calculated:

$$d(H) = \frac{kT}{3\pi\eta D} \quad (6.1)$$

The hydrodynamic diameter is dependent on Boltzmann's constant (k), the absolute temperature (T), the viscosity of the solvent (η) and the translational diffusion coefficient (D). The hereby obtained diameter is the one according to a sphere with the same translational diffusion coefficient as the particle (figure 6.1). Ionic strength of the solution also affects the diffusion speed. A medium possessing a low conductivity produces an extended double layer of ions around the particle. This reduces the diffusion speed and leads to a higher apparent hydrodynamic diameter. Adsorbed species, such as polymers, will also influence the measurand. If the adsorbed species protrudes over the particle, the diffusion speed decreases to a higher extent than it would if it was close to the particle's surface. The measurement is accomplished by irradiating the sample with laser light. In an angle of 173° the backscattered light is detected. The gained information is a speckle pattern. If, theoretically, the particles in solution do not move at all, this speckle pattern would be identical over the time. In praxis, the particles move. This is yielding in a change of this pattern. The correlation of the patterns over time are recorded and provide a correlogram. The faster the decay time is, the smaller are the particles. This information can be converted into a size distribution of the particles.

6.2 Zeta potential

Zeta potential is a measurand which can help to predict the tendency of aggregation of particles in a particular environment. It does not describe the charge of a particle itself,

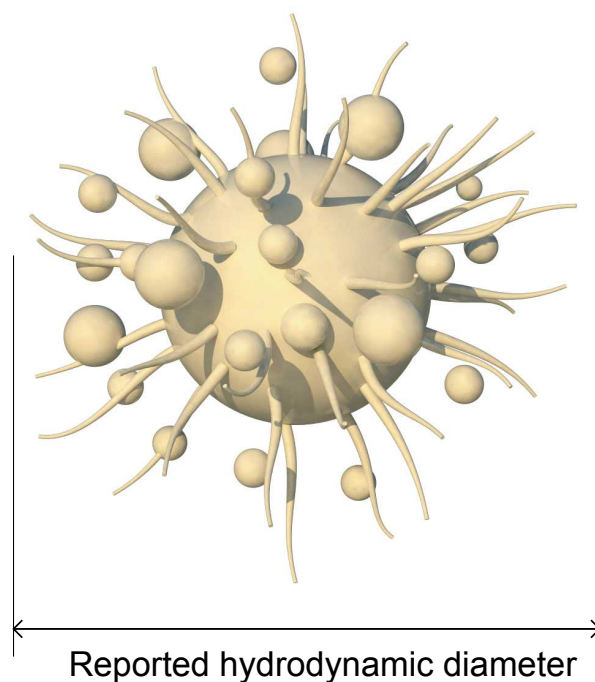


Figure 6.1: The hydrodynamic diameter of a particle with functional groups and adsorbed ions.

but the potential of the slipping plane in this media. Nearly every particle in solution is surrounded by a layer of ions. The ions which are in close contact to the particle are attached to it. When the particle moves, the ions perform the exact same motion. Zeta potential is measured at the outer part of this layer, where the attached ions pass the bulk solution. Zeta potential is extremely dependent not only on the particle charge but also on the composition of the medium in which the particles are dispersed. Particles with high zeta potentials (i.e. <-30 mV and $>+30$ mV) will repel each other and form a stable dispersion. The measurement of zeta potential is based on laser Doppler anemometry (LDA). Particles in solution are exposed to an electric field. They will move towards the electrode of opposite charge in a velocity proportional to the magnitude of the zeta potential. The movement of the particles is determined by the frequency shift or phase shift an incident laser beam experiences.

Part III

Experimental section

7 Materials

The devices, chemicals and materials used in this thesis are listed in table 7.2 and 7.1.

Table 7.1: Devices used for this thesis.

Device	Supplier
calflex filter	Schott, Germany
Cary50 UV-VIS spectrophotometer	Varian, US
digital mass flow controller	MKS, Germany
DSC-830 lock-in amplifier	Stanford Research Inc., Germany
F-7000 Fluorimeter	Hitachi, Germany
microx TX3	PreSens, Germany
ph-1 mini	PreSens, Germany
RG9 filter	Schott, Germany
ROTOFIX32 centrifuge	Hettich-Zentrifugen, Germany
Optima LE-80K Ultracentrifuge	Beckman Coulter, Germany

Table 7.2: Chemicals used for this thesis.

Chemical	Abbr.	Supplier	Comments
CHEMICALS AND SOLVENTS			
1-octadecen		Sigma-Aldrich	$\geq 90\%$
2,2'-Azobis(2-methylpropionitrile)	BIS	Acros Organics	98%
(4-allylaminocarbonylphenyl)boronic acid	BA	Combi Blocks Inc.	97%
acrylamide	AAM	Acros Organics	98.5%
cadmium oxide	CdO	Sigma-Aldrich	$\geq 99.99\%$
ethanol	EtOH	Roth	synthesis grade
magnetite nanoparticles developer kit		Ferro Tec	
<i>N</i> -isopropylacrylamide	NIPAAm	Acros Organics	98%
oleic acid		Sigma-Aldrich	$\geq 90\%$
oxacyclopentan	THF	Roth	synthesis grade
potassium peroxodisulfate	PPS	Roth	$\geq 94\%$
selenium	Se	Sigma-Aldrich	$\geq 99.5\%$
sodium dodecylsulfate	SDS	Fluka	$\geq 98\%$
trioctylphosphine	TOP	Sigma-Aldrich	techn. 90%
GASES			
nitrogen	N ₂	Air Liquide	$\geq 99.999\%$
oxygen	O ₂	Linde	0.1% O ₂ in N ₂
synthetic air		Air Liquide	
POLYMERS			
poly(styrene- <i>co</i> -maleic anhydride)	EF-80	Sartomer	
poly(styrene- <i>co</i> -maleic anhydride)	PSMA93	Sigma-Aldrich	
DYES			
acryloylpiperazinyl sulforhodamine B isomer	ASRB		46
Brilliant Blue FCF		Ringe Kuhlmann	
<i>N</i> -fluorescein-acrylamide	FLAC		46
Iridium (III)((benzothiazol-2-yl)-7-(diethylamino)-cumarin) ₂ (acetylacetonat)	Ir(Cs) ₂ (acac)		47
Palladium (II) meso-tetra(4-fluorophenyl)-tetrabenzoporphyrin	PdTPTBPF		48
Platinum (II) meso-tetra(4-fluorophenyl)-tetrabenzoporphyrin	PtTPTBPF		48

8 Core synthesis

8.1 Core precipitation

The precipitation of the core particles always followed the same pattern. A cocktail was fabricated, containing the desired concentrations of the components. These are listed in table 8.1 and 8.2. The solvent of the cocktail was tetrahydrofuran (THF). THF was used as it is miscible with water but not a solvent for the PSMA. The polymer concentration is indicated in weight percent of the organic solvent, thus THF. The two polymer types used were the polystyrene-maleic anhydride co-polymers EF-80 and PSMA93. Their molecular weight and the MA content is listed in table 8.3. The concentration of magnetite and dyes is indicated in weight percent of the polymer concentration. The two possible directions of precipitation are CiP (cocktail into precipitant) and PiC (vice versa). At CiP, for example, the precipitant is vortexed, while the cocktail is added. Three different vortex velocities were used: 600, 1200 and 1800 rpm. The flow rate is indicated as S (0.04 mL s^{-1}), M (0.5 mL s^{-1}) and F (2 mL s^{-1}). After precipitation, the THF is evaporated by compressed-air.

Table 8.1: Instructions for the precipitation of the core particles. Part 1

Core indication	V_{cocktail} (mL)	$V_{\text{precipitant}}$ (mL)	Polymer conc. (wt%)	Magnetite (wt%)	Polymer	CiP / PiC	Vortex velocity (rpm)	Flow rate (S, M, F)
EC1	0.5	4.5	0.2	20	EF-80	CiP	1,200	M
EC2	0.5	4.5	0.4	20	EF-80	CiP	1,200	M
EC3	0.5	4.5	0.6	20	EF-80	CiP	1,200	M
EC4	0.5	4.5	0.8	20	EF-80	CiP	1,200	M
EC5	0.5	4.5	1.0	20	EF-80	CiP	1,200	M
EC6	0.5	4.5	1.2	20	EF-80	CiP	1,200	M
PC1	0.5	4.5	0.2	20	PSMA93	CiP	1,200	M
PC2	0.5	4.5	0.4	20	PSMA93	CiP	1,200	M
PC3	0.5	4.5	0.6	20	PSMA93	CiP	1,200	M
PC4	0.5	4.5	0.8	20	PSMA93	CiP	1,200	M
PC5	0.5	4.5	1.0	20	PSMA93	CiP	1,200	M
PC6	0.5	4.5	1.2	20	PSMA93	CiP	1,200	M
EP1	0.5	4.5	0.2	20	EF-80	PiC	1,200	M
EP2	0.5	4.5	0.4	20	EF-80	PiC	1,200	M
EP3	0.5	4.5	0.6	20	EF-80	PiC	1,200	M
EP4	0.5	4.5	0.8	20	EF-80	PiC	1,200	M
EP5	0.5	4.5	1.0	20	EF-80	PiC	1,200	M
EP6	0.5	4.5	1.2	20	EF-80	PiC	1,200	M
EV1	0.5	4.5	0.6	20	EF-80	CiP	600	M
EV2	0.5	4.5	0.6	20	EF-80	CiP	1,200	M
EV3	0.5	4.5	0.6	20	EF-80	CiP	1,800	M
PV1	0.5	4.5	0.6	20	PSMA93	CiP	600	M
PV2	0.5	4.5	0.6	20	PSMA93	CiP	1,200	M
PV3	0.5	4.5	0.6	20	PSMA93	CiP	1,800	M

Table 8.2: Instructions for the precipitation of the core particles. Part 2

Core indication	V _{cocktail} (mL)	V _{precipitant} (mL)	Polymer conc. (wt%)	Magnetite (wt%)	Polymer	CiP / PiC	Vortex velocity (rpm)	Flow rate (S, M, F)
EF1	0.5	4.5	0.6	20	EF-80	CiP	1,200	S
EF2	0.5	4.5	0.6	20	EF-80	CiP	1,200	M
EF3	0.5	4.5	0.6	20	EF-80	CiP	1,200	F
PF1	0.5	4.5	0.6	20	PSMA93	CiP	1,200	S
PF2	0.5	4.5	0.6	20	PSMA93	CiP	1,200	M
PF3	0.5	4.5	0.6	20	PSMA93	CiP	1,200	F
PM1	0.5	4.5	0.6	5	PSMA93	CiP	1,200	M
PM2	0.5	4.5	0.6	10	PSMA93	CiP	1,200	M
PM3	0.5	4.5	0.6	20	PSMA93	CiP	1,200	M
PM4	0.5	4.5	0.6	30	PSMA93	CiP	1,200	M
EIr ¹	5	10	0.5	20	EF-80	CiP	1,200	M
PPd ²	5	10	0.6	20	PSMA93	CiP	1,200	M
PPt ³	5	10	0.6	20	PSMA93	CiP	1,200	M
PH	5	10	0.5	20	EF-80	CiP	1,200	M
SU	5	10	0.5	20	EF-80	CiP	1,200	M
DD	5	10	0.5	20	EF-80	CiP	1,200	M

¹2 wt% Ir(Cs)₂(acac)²1.5 wt% PdTPTBPF³1.5 wt% PtTPTBPF

Table 8.3: Properties of EF-80 and PSMA93.

Polymer	Molecular weight (g mol ⁻¹)	MA content (wt%)
EF-80	14,400	11
PSMA93	224,000	7

8.2 K_{SV} measurements

For all three measurements, a mass flow controller was used to blend the gases in order to obtain the desired concentration. As this hardware is known to be error-prone, the actual oxygen content in the solution to be measured was recorded by a Microx TX3 of PreSens. In every experiment three runs were carried out.

8.2.1 Ir(Cs)₂(acac)

The EIr particles were characterized with a pH-mini device of PreSens, which is adaptable for the luminescence of Ir(Cs)₂(acac). The modulation frequency was 20,000 Hz. As gases, nitrogen and synthetic air were used. The range of 0 to 100 % airsaturation was measured in steps of 10 %. One measurement at 25°C and one at 40°C was conducted.

8.2.2 PtTPTBPF and PdTPTBPF

For the characterization of PPd and PPt particles, a lock-in amplifier was utilized. For excitation a LED of 630 nm with a Calflex filter was used. The filter for the PMT was a RG9 filter. The settings of the lock-in amplifier are listed in table 8.4. PPt was characterized for 0 to 100 % airsaturation in steps of 10 %. The used gases were nitrogen and synthetic air. As PPd is a trace oxygen sensor, the characterization was done for 0 to 5 % airsaturation. For this purpose, nitrogen and a test gas with 1 % oxygen were used.

Table 8.4: Settings of the lock-in amplifier.

Parameter	PPt	PPd
modulation frequency (Hz)	5,000	700
amplitude (V)	5	5
time constant (ms)	3	3
sensitivity (mV/mA)	50	50
low pass filter slope (dB/oct)	18	18

9 Shell synthesis

The polymerization was carried out according to the following procedure with minor variations. Typically, 10 mL of deionized water were provided in a round bottom flask. 50 mg of either NIPAAm or AAm, 2.5 *mol%* BIS, and 12 mg boronic acid were dissolved in the water. In case emulsifier was used, the concentration of SDS was 1.25 mM. 0.24 mg *N*-fluorescein-acrylamide and 0.25 mg acryloylpiperazinyl sulforhodamine B isomer were dissolved in 2 mL of ethanol and added to the round bottom flask. This mixture was stirred, heated and flushed with nitrogen for 15 min (reaction with SDS) or 45 min (reaction without SDS). The polymerization was started by the addition of PPS (12 mg for a reaction with SDS, 3 mg for a reaction without SDS dissolved in 1 mL deionized water) and maintained under continuous stirring for 60 min. Thereafter, the synthesized particles were transferred into a vial and separated by a magnetic field. After collection, the supernatant was removed and fresh deionized water was added. This washing step was repeated two more times. The used quantities for the polymerization are listed in table 9.1.

Table 9.1: Utilized quantities of reagents for shell polymerization.

Particles	Core	Core (mg)	Monomer	Monomer (mg)	SDS (mM)	BIS (mol%)	FLAC (mg)	ASRB (mg)	BA (mg)	PPS (mg)
EIrP	EIr	18	NIPAAm	50	1.25	2.5				12
PHP	PH	15	AAm	64		15	0.24	0.45		3
SUP1	SU	15	NIPAAm	50	1.25	2.5	0.16			12
SUP2	SU	15	NIPAAm	50		2.5	0.24	0.45	12	3
DLP1	DD	15	NIPAAm	50	1.25	2.5				12
DLP2	DD	15	NIPAAm	50	1.25	5.2				12
DLP3	DD	15	NIPAAm	50	1.25	9				12
DLP4	DD	15	NIPAAm	50		9				6
DLP5	DD	15	NIPAAm	50		9				3
DLP6	DD	15	NIPAAm	50		15				3

10 Quantum dot synthesis

The synthesis of the quantum dots was carried out according to a publication of Boatman.⁴⁹

10.1 QD synthesis

Preparation of the precursor. 39 mg of selenium, 5 mL octadecene and 0.4 mL of tri-octylphosphine were provided in a round bottom flask. The dispersion was stirred and heated until the selenium was dissolved. After cooling down to room temperature, the solution was transferred into a sealed container.

QD synthesis. 13 mg of cadmium oxide, 0.6 mL oleic acid and 10 mL octadecene were provided in a flask equipped with a thermometer. The solution was heated to 225°C, then 1 mL of the precursor was added. After 5 to 240 seconds the reaction was stopped by transferring the mixture into a crystallizing dish which was precooled with liquid nitrogen.

Isolation of the QDs. The suspension was transferred to a micro centrifuge tube and covered with ethanol. After shaking, the emulsion was separated by centrifugation (3,000 rpm for 5 min). The supernatant was removed. This procedure was repeated twice.

10.2 Determination of the quantum yield

The determination of the quantum yield was done with a reference method. For this method, a reference dye with a known (and high) quantum yield and a similar absorption maximum is required. A solution of the reference dye as well as of the sample are prepared, both showing an absorption of approximately 0.05 up to 0.1. Emission spectra are recorded of these solutions. The excitation light has to be monochromatic. After correction of the PMT sensitivity, the spectra are plotted, smoothed and the background is subtracted. Now, the integrals of the two spectra can be calculated. With equation 10.1 the quantum yield of the sample can be evaluated. The index R indicates the values for the reference dye, ϕ is the quantum yield, Int the integral of the spectrum, A the absorption of the sample and n the refractive index of the solvent.

$$\phi = \phi_R \frac{Int}{Int_R} \frac{A_R}{A} \frac{n^2}{n_R^2} \quad (10.1)$$

Part IV

Results and discussion

11 Synthesis and characterization of core-particles

As the aim of this thesis was to generate magnetic optical sensor particles (MOSePs) in a core-shell approach, first of all the core had to be synthesized. All core particles were obtained by nano-precipitation of the polymers EF-80 and PSMA93. They are polymers of different molecular weight and composition, consisting both of poly(styrene-co-maleic anhydride) (PSMA). The general procedure is explained in part III, chapter 8. These core particles can be functionalized by incorporation of nano-scaled magnetite particles or indicator dyes. Doing so, magnetic oxygen-sensitive sensor particles can be obtained, for example.

11.1 Influence of precipitation-parameters on the particle sizes

In the course of nano-precipitation of the core-particles, some parameters can be varied to adjust the size of the particles. Here, the influence of the parameters is discussed.

11.1.1 Polymer concentration

First of all, the concentration of polymer in the cocktail can be varied. Therefore, cocktails with polymer contents from 0.2 to 1.2 *wt%* of both polymers were used for precipitation. EF-80 has, compared to PSMA93, shorter chains and hence a higher molecular weight. It also possesses a higher maleic anhydride (MA) content, resulting in a higher polarity of the material (table 11.1).

Table 11.1: Characteristics of EF-80 and PSMA93

Polymer	Molecular weight (g mol ⁻¹)	MA content (<i>wt%</i>)
EF-80	14,400	11
PSMA93	224,000	7

The hydrodynamic radius (z-average) and polydispersity index (PDI) of the obtained particles were measured by dynamic light scattering. Figure 11.1 shows the correlation between polymer concentration in the cocktail or the polymer type, respectively, and the particle size. The higher the polymer concentration in the cocktail was, the higher were the hydrodynamic diameters. This is valid for both polymer types and the effect is a significant one. Therefore, the polymer concentration is a valuable parameter for adjusting particle size. It can be seen that particles made of PSMA93 are approximately 40 nm bigger than those made of EF-80. This is probably a result of the higher molecular weight of PSMA93, yielding in a higher viscosity of the cocktail. The high viscosity leads to formation of bigger particles. Additionally,

the higher polarity of EF-80 favors the polymer-precipitant interactions, yielding in smaller particles.

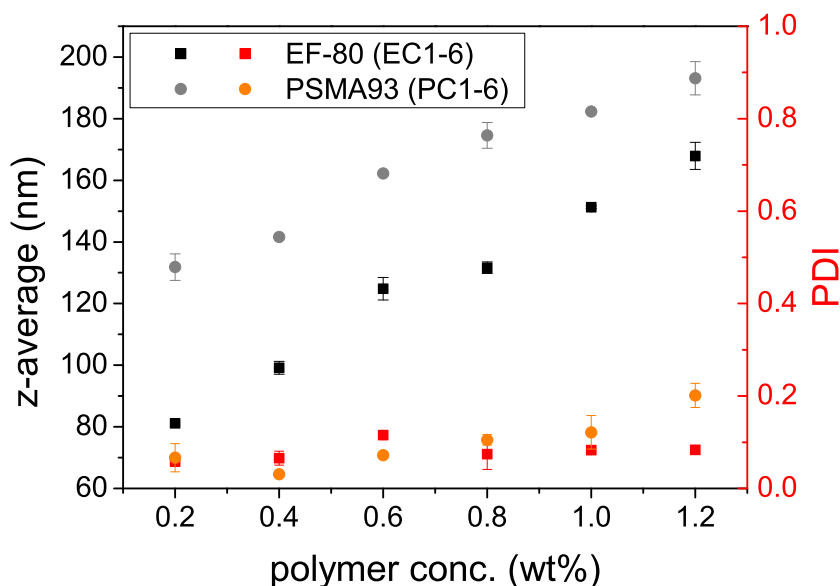


Figure 11.1: Dependency of z-average on polymer type and concentration in the cocktail, respectively.

11.1.2 Direction of precipitation

There are two possibilities to accomplish the precipitation. Either the cocktail is poured into the precipitant (CiP) or the precipitant is injected into the cocktail (PiC). The precipitation behavior was examined with cocktails of different polymer concentrations of type EF-80. The core particles fabricated by CiP method were 20 to 50 nm smaller, as a faster dilution of the cocktail occurs. In contrast, applying the other direction (PiC), the cocktail experiences a slower dilution. There is more time available to form particles of a lower, thus favored, surface/volume ratio (figure 11.2).

11.1.3 Vortex speed

The vortex speed did not have an influence on particle size. Again, cocktails of both polymers were prepared and precipitation was carried out with three different vortex speeds (figure 11.3). Mixing seems to be sufficient already at 600 min^{-1} , either because of the vortex or the cocktail injection itself.

11.1.4 Flow rate of cocktail addition

The velocity of cocktail injection also has an influence on particle size, although not a very significant one. Three flow rates of cocktail addition were tested:

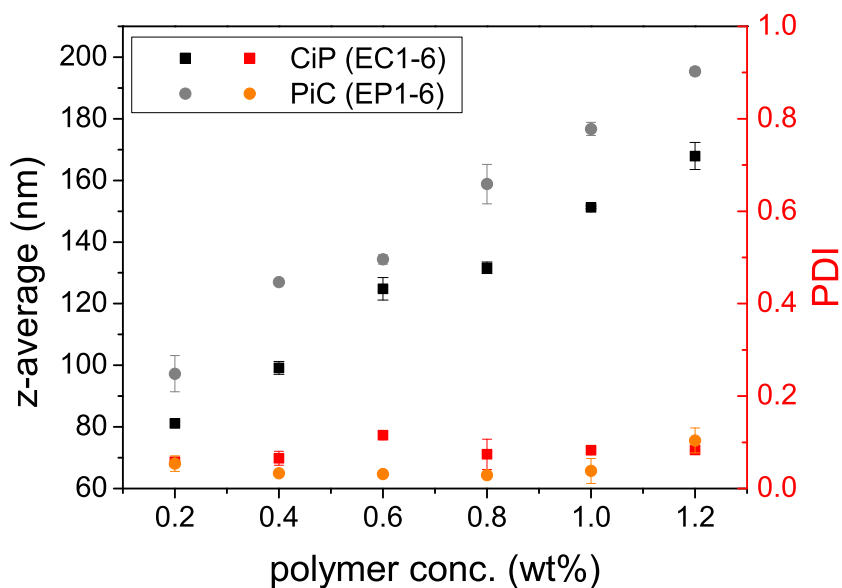


Figure 11.2: Influence of the precipitation direction (CiP/PiC) on the particle size.

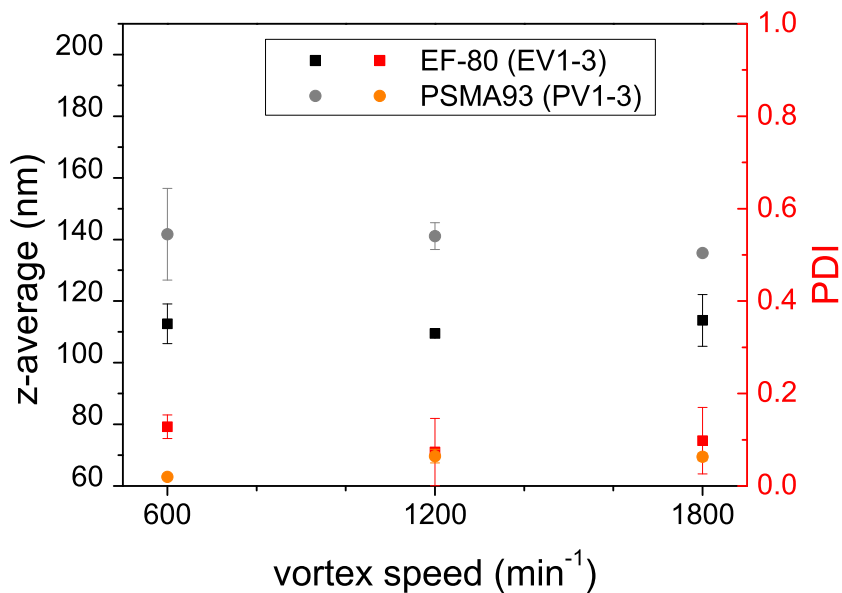


Figure 11.3: Particle sizes at different vortex speeds.

- S for slow (one drop per second)
- M for medium
- F for fast (the fastest way possible using a sampler).

Figure 11.4 shows a slight dependency of the flow rate. The faster the cocktail was added, the smaller the resulting particles were.

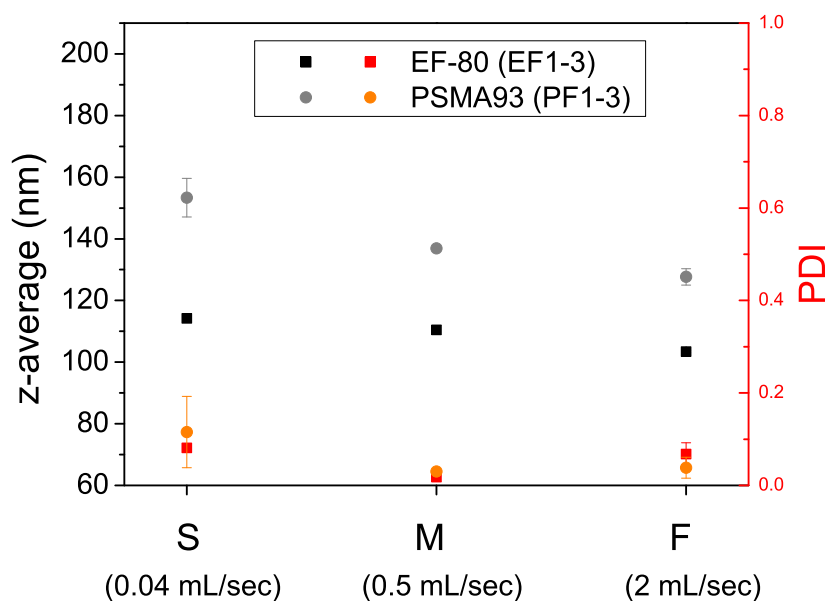


Figure 11.4: The effect of cocktail injection velocity on z-average.

11.1.5 Magnetite concentration

As last parameter, the magnetite concentration was examined. By increasing the magnetite concentration in the cocktail, the particle size decreased (figure 11.5). This effect can be explained by the assumption that magnetite particles act as seeds for the polymeric particles. When a higher amount of magnetite is available, more particles with smaller sizes develop.

In summary, most effect on particle size have polymer concentration, polymer type and magnetite concentration. The z-average of the particles can be adjusted in the range between 80 and 190 nm. While for medical application smaller sizes are favored, particles for magnetic separation should possess a z-average value of at least 100 nm. This ensures reasonable collection times for measurements.

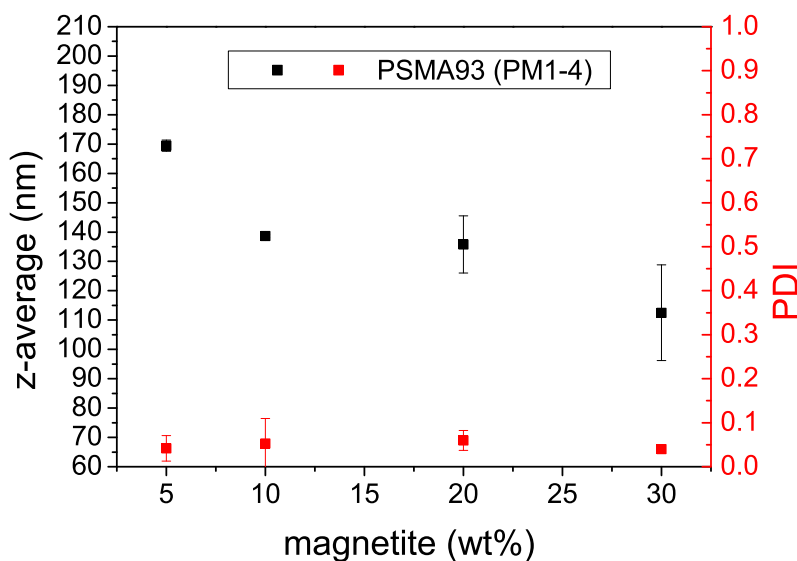


Figure 11.5: The magnetite concentration in the cocktail has an impact on the hydrodynamic diameter of the particles.

11.2 Functionalization of core particles

With the incorporation of magnetite, a first functionality was already introduced. Next to magnetism, also sensing properties can be applied by including indicator dyes into the particles. The procedure is the same as with magnetite. All desired components are added to the cocktail which then is precipitated. During this thesis, three different oxygen sensitive fluorescent indicators were incorporated and calibration curves of the achieved MOSePs were recorded.

11.2.1 Ir(Cs)₂(acac)

At first, core particles with the oxygen sensitive dye iridium (III)((benzothiazol-2-yl)-7-(diethylamino)-cumarin)₂(acetylacetonat) or Ir(Cs)₂(acac) (figure 11.8) were precipitated (EIr). This indicator can be used to produce sensors with a high dynamic range. ($pO_2=0-1,000$ hPa)² Such sensors are ultra bright oxygen optodes⁴⁷ with absorption and emission maxima both within the VIS spectrum (table 11.2). Additionally, a shell of pNIPAAm was polymerized around these EIr core particles. The characterization data can be found in chapter 13 on page 59.

11.2.2 PtTPTBPF

Also, platinum (II) meso-tetra(4-fluorophenyl)tetrabenzoporphyrin (PtTPTBPF) was incorporated (with Pt as metal ion (M), figure 11.8 shows the indicator dye). With a decay time of 50 μ s, it can be used as oxygen sensor. In table 11.2 the photo-physical properties can be seen. This dye is highly photo-stable, allowing long-time measurements with high light

densities.⁴⁸ The phosphorescence emission is in the near-infrared, providing a lower absorption of the emitted light by the included magnetite compared to Ir(Cs)₂(acac), for example. The precipitated PSMA93 particles containing magnetite and PtTPTBPF (PPt) are capable of monitoring oxygen from 0 - 100 % airsaturation. Applying the simplified two-site model (equation 2.7) the quenchable fraction was determined as $f_1=0.93$ with a quenching constant of $K_{SV1}=0.016 \text{ hPa}^{-1}$. The Stern-Volmer plot can be seen in figure 11.6.

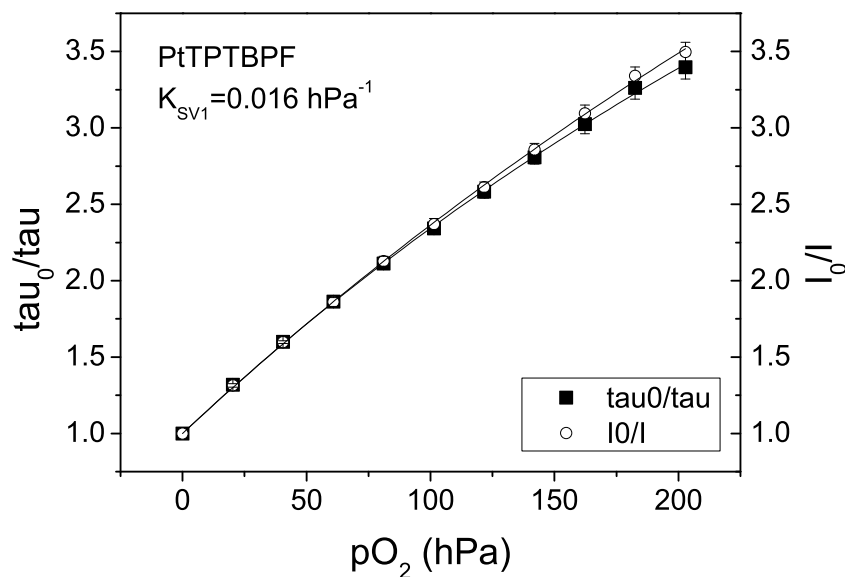


Figure 11.6: Stern-Volmer plot of PtTPTBPF ($K_{SV1}=0.016 \text{ hPa}^{-1}$, $f_1=0.93$).

11.2.3 PdTPTBPF

Another very photo-stable dye is palladium (II) meso-tetra(4-fluorophenyl)tetrabenzoporphyrin (PdTPTBPF) (with $M=\text{Pd}$, figure 11.8 shows the structure) which is also emitting in the near-infrared. This indicator is qualified to be used for trace oxygen monitoring. Incorporated in magnetic PSMA93 particles (PPd), a calibration curve from 0 - 5 % airsaturation was done. Application of the simplified two-site model (equation 2.7) showed a quenchable fraction f_1 of 0.89 with a K_{SV} of 0.067 hPa^{-1} (figure 11.7).

Table 11.2: Photo-physical properties of the used indicators.

Dye	Abs _{max} (nm)	Em _{max} (nm)	τ (μs)
Ir(Cs) ₂ (acac)	446; 475	564; 611	11
PtTPTBPF	431; 565; 615	773	50
PdTPTBPF	443; 579; 629	803	297

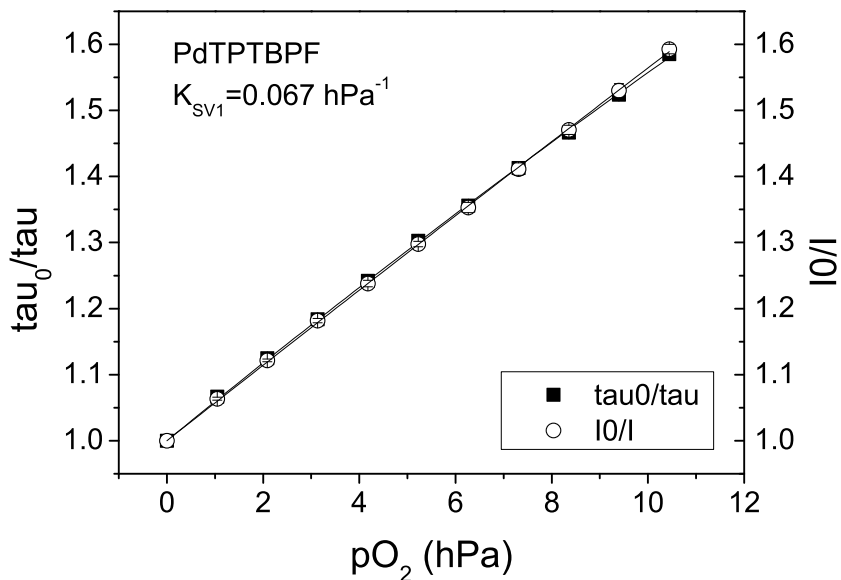


Figure 11.7: Stern-Volmer plot of PdTPTBPF ($K_{SV1}=0.067 \text{ hPa}^{-1}$, $f_1=0.89$).

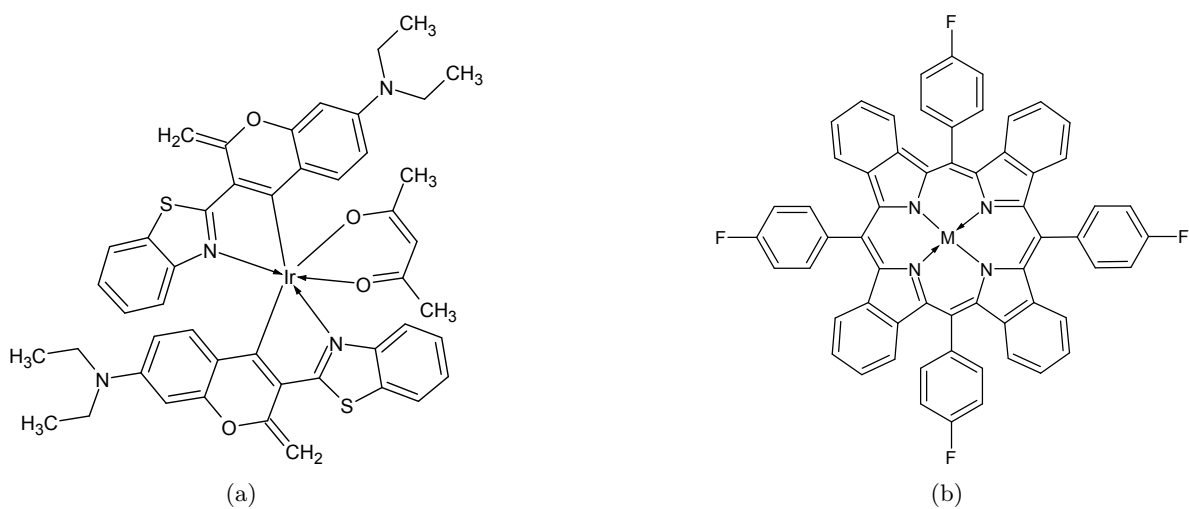


Figure 11.8: Structures of $\text{Ir}(\text{Cs})_2(\text{acac})$ (a) and PtTPTBPF (M=Pt) and PdTPTBPF (M=Pd), respectively (b).

12 Synthesis and characterization of quantum dots

Another attempt to functionalize the core particles was to incorporate quantum dots (QDs). QDs are semiconducting materials with sizes smaller than the Bohr exciton diameter of that material. Such quantum dots are beads of sizes between 1 and 100 nm. They possess very astonishing optical properties, such as a very broad absorption band as well as a narrow, tunable emission band. Also, they are considered to have high quantum yields and an extremely high photostability. These attributes seem to make them suitable for light harvesting purposes. By incorporating quantum dots with specified emission maxima into the core, they can be excited by one single wavelength of high energy. This energy can be passed to acceptor dyes in the shell of the particles, either by radiative or non-radiative energy transfer. Using this setup, a range of sensitive dyes can be excited simultaneously by an initial irradiation of only one wavelength. QD materials often consist of selenium and cadmium, both being toxic to humans. For this reason a proper protective coating is required. The additional shell consisting of either poly(acrylamide) or pNIPAAm can act as a shield to prevent direct contact of the quantum dots with the surrounding area.

12.1 Influence of the reaction time on the emission wavelength

As described in chapter 4, the emission wavelength of quantum dots is dependent on their size. The larger the quantum dots are, the longer is the wavelength of the emitted light. The size again is dependent on the reaction duration, as the crystals grow larger with time. For that reason, it is possible to produce tailor-made quantum dots with a desired emission wavelength. Figure 12.1 shows the maximum emission wavelength of the synthesized quantum dots in correlation to the reaction time. Producing quantum dots by the instructions given in chapter 10, emission maxima in the range of 490 to 585 nm can be achieved.

12.2 Characterization of the produced QDs

Next to the emission maxima also the quantum yields and characteristics of absorption and excitation are of interest. For that reason, a more in-depth characterization of four batches was done. First of all, emission and absorption spectra were recorded. Figure 12.2 shows the absorption, excitation and emission spectra of the batch qd01. In theory, the maximum of the excitation is the same as the maximum of the absorption. It is noticeable that here a discrepancy of 5 nm occurs. A possible reason for this is an overlay of the specific QD absorption with some unspecific absorption resulting from impurities. The discrepancy of absorption and excitation maximum was found in every batch. The purification of the synthesized QDs was not completely possible. The QDs are coated unspecifically by organic residues. They seem to be responsible for stability and, maybe more important, for dispersibility of the QDs.

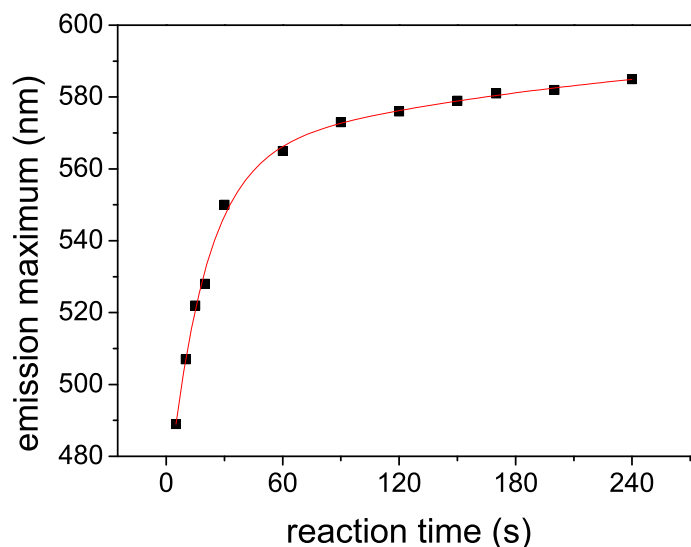


Figure 12.1: The dependency of the emission maximum of the synthesized quantum dots on the reaction time.

One attempt was taken to further purify the QDs resulting in an insoluble residue, which has lost its ability to emit light. Whether no light was emitted because the quantum dots were degenerated in some way or because self quenching occurred due to the high concentration could not be tested. Anyhow, according to an elementary analysis, the portion of cadmium and selenium in the processed QDs is only 3.5%. This contingent was raised to 10% when further purification was applied. The Stokes shifts of the quantum dots are between 9 and 14 nm referred to the data of the excitation spectra. The data of the excitation spectra is considered to be more specific than the absorption spectra. For excitation spectra only the emitted light by the QDs is measured whereas the absorption spectra may also show unspecific absorption of impurities in the sample. Therefore, a superposition of the absorbance of QDs and other materials can occur. This might be the reason for the observed shift of the maxima recorded by excitation or absorption.

An extinction coefficient ϵ was also determined. Because of the above mentioned reasons neither the molar mass of the QDs nor the concentration of QDs in the processed sample was known. Therefore, only a relative comparison using a weight-related extinction coefficient was possible. The absorption of calibration solutions, based on the weight of the samples, were measured. The obtained slope yielded in an extinction coefficient in the dimensions of $\text{mL mg}^{-1} \text{cm}^{-1}$. This approximation is only a vague estimation of the coefficient. In table 12.1 the optical properties are listed. The increasing values for ϵ correlate with longer reaction times. A higher content of absorbing organic impurities induced by a longer exposure to heat could be the reason for increasing values of the extinction coefficient.

Using the technique described in chapter 10 the quantum yield ϕ was determined. Surprisingly, the quantum yields were between 2 and 8%. Even though no values for quantum yields of QD could be found in literature so far, QDs are known for their supposed high brightness.

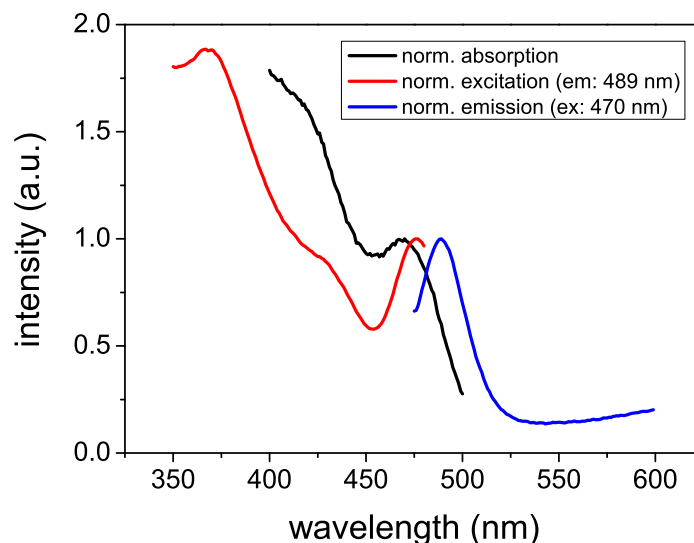


Figure 12.2: Normalized absorption, excitation and emission spectra of qd01. The excitation spectrum was recorded at a wavelength of 489 nm. The excitation wavelength for the emission spectrum was 470 nm.

Astonished by the results of this analysis, a comparison with commercially available quantum dots was done.

Table 12.1: Emission and absorption maxima as well as quantum yields (ϕ) of some synthesized QDs.

QD	Abs _{max} (nm)	Exc _{max} (nm)	Em _{max} (nm)	ϕ (%)	ϵ (mL mg ⁻¹ cm ⁻¹)
qd01	470	476	489	8	0.02794
qd02	505	512	522	5	0.04247
qd03	506	515	529	5	-
qd04	508	516	525	2	0.25005

12.3 Comparison of the synthesized quantum dots to commercially available QDs

The commercially available QDs “EviDot Jonamac Red” were used for comparison. No data sheet for this product was available. The only information on the package was the concentration of the dispersion. As every quantum dot has a shell which changes the weight of the particle, we did not know whether the given concentration was calculated by the weight of the pure QDs or by the weight of the QDs with the coating. In order to make the synthesized QDs comparable to the bought ones, three solutions of qd03 with different concentrations

were provided (table 12.2). The aim was to obtain one solution with the same concentration like the EviDot solution. In order to allow comparison, the extinction coefficients of the EviDots and the synthesized QDs were considered to be similar. Therefore, the obtained information is only a rough estimation, but the only way possible to gain insight. The EviDot solution with a concentration of 0.25 mg mL^{-1} was prepared using the weight indication on the package. The solutions qd03a-c were prepared using the weighted sample, the corresponding amount according to 100 % theoretical conversion and to 3.5 % CdSe content determined by elementary analysis. Absorption, excitation and emission spectra with the same settings were recorded using these four solutions. Furthermore, the quantum yield of the EviDots was determined.

Table 12.2: Concentrations of the QD solutions. One of the qd03 solutions was meant to have the same concentration as the EviDot solution.

Solution	Initial sample (mg/mL)	Desired conc. (mg/mL)	Comment
EviDot	0.25	0.25	concentration stated on the package
qd03a	0.25	0.25	weight based on the processed sample
qd03b	2.80	0.25	weight based on 100 % theoretical conversion
qd03c	7.14	0.25	weight based on 3.5 % QD content calculated by elementary analysis

In the absorption spectra (figure 12.3) it can be seen, that the maximum of absorption is at 505 nm for qd03 and at 640 nm for EviDot. Furthermore, the maximum is more distinct for qd03. Regarding the absorption, the solution qd03b (which was prepared using 100 % of theoretical conversion) has a similar concentration of QDs as the EviDot solution. A look on the emission spectra (figure 12.4) reveals that solution qd03c is already of such a high concentration that inner filter effects occur. Referring to the emission spectra it seems that the actual concentration of EviDot lies in between the concentration of qd03b and qd03c. The excitation spectra (figure 12.5) also affirm this assumption.

The quantum yield of the EviDots was determined as 13.2%. Compared to the one of qd03, which was 5%, the commercially available QDs do not possess significantly better optical properties. Knowing that, it seems that QDs actually are excitable in a broad range of the spectrum but do not possess the extreme brightness they are propagated for.

12.4 Incorporation of QDs in a sensor foil

To verify whether the synthesized quantum dots can act as a donor for Förster resonance energy transfer (FRET) foils were produced. As acceptor dye MACROLEX Fluorescent Red G (MFR) was introduced. Its absorption maximum overlaps very well with the emission maximum of the qd05. This is, next to the proximity, one of the most important conditions for FRET. Four foils of a thickness of $3.75 \mu\text{m}$ were coated with a doctor knife. One consisted only of poly(styrene) which was used as the blind for absorption measurement. Two other foils additionally contained 1 wt% of either qd05 or MFR and the last one had 1 wt% of both dyes. Figure 12.6 shows the absorption spectra of the foils. It is peculiar that the absorption maximum of the QDs can not be seen in the absorption spectrum. As soon as the QDs are

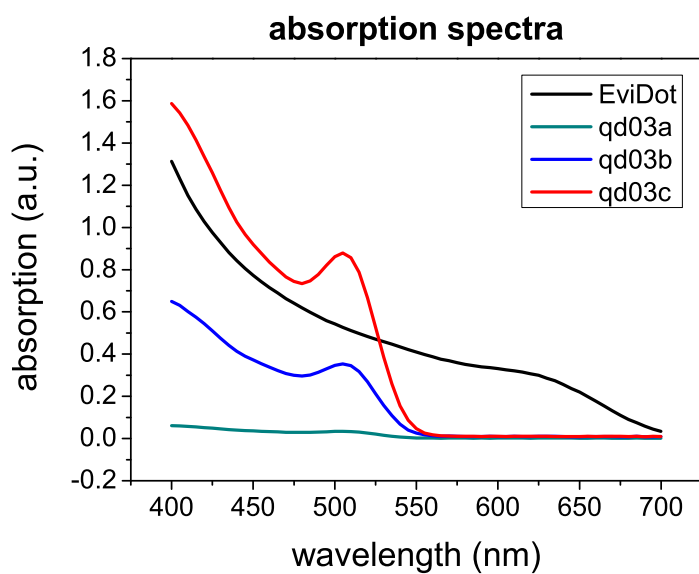


Figure 12.3: Absorption spectra of EviDot and qd03 (different concentrations).

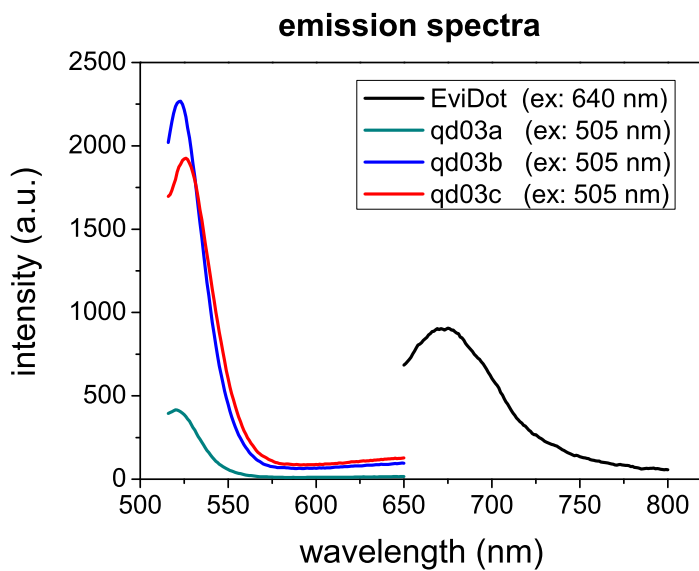


Figure 12.4: Emission spectra of EviDot and qd03 (different concentrations). The excitation wavelength was 640 nm and 505 nm, respectively.

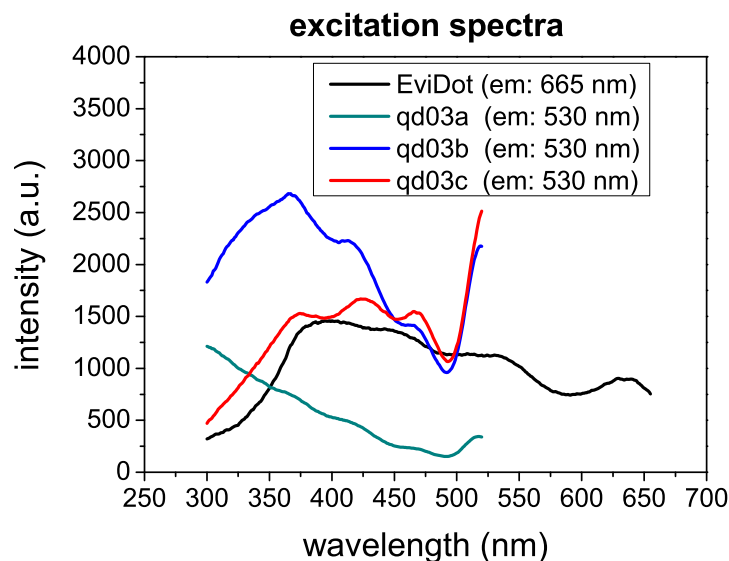


Figure 12.5: Excitation spectra of EviDot and qd03 in different concentrations. The emission at wavelengths of 665 nm and 530 nm was recorded.

not in solution, the peak disappears from the absorption spectrum. Anyhow, the spectra validate the successful incorporation of the dyes into the foil. The emission spectra (figure 12.7) confirm a FRET. It can be seen that the emission of MFR is more than three times higher with qd05 in its surrounding, while the emission of qd05 at 520 nm is completely missing. Unfortunately, this was the only foil where the QD emission, respectively a FRET, could be seen. In every subsequent one only noise and scattering were visible. Obviously the first time I had luck. But exploring the reason why the introduction of QD into a foil works out or not would have been out of proportion for this thesis.

12.5 Incorporation of QDs in particles

Precipitation of particles in presence of QDs was also done. But here again, neither absorption maximum nor emission of QDs could be verified. The adaption of QDs on my particles was not possible in a reasonable time scale. This is why the excursus on quantum dots stops here.

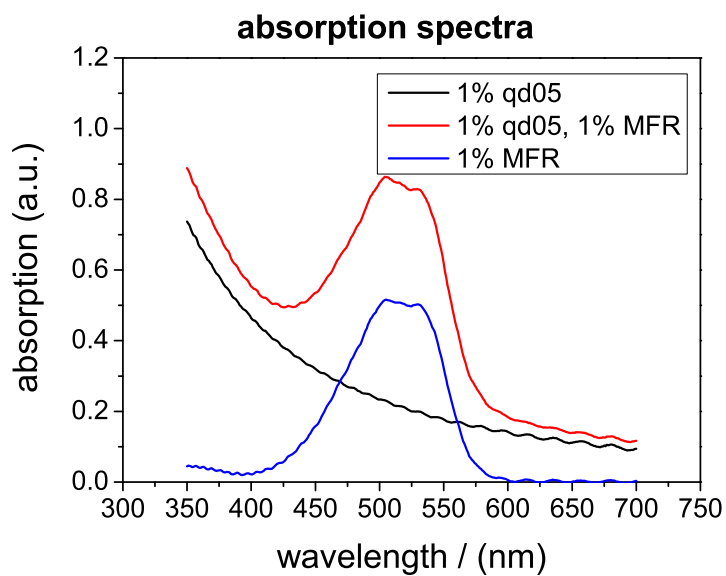


Figure 12.6: Absorption of foils with qd05 (1%), MACROLEX Fluorescent Red G (MFR) (1%) and both (1% each).

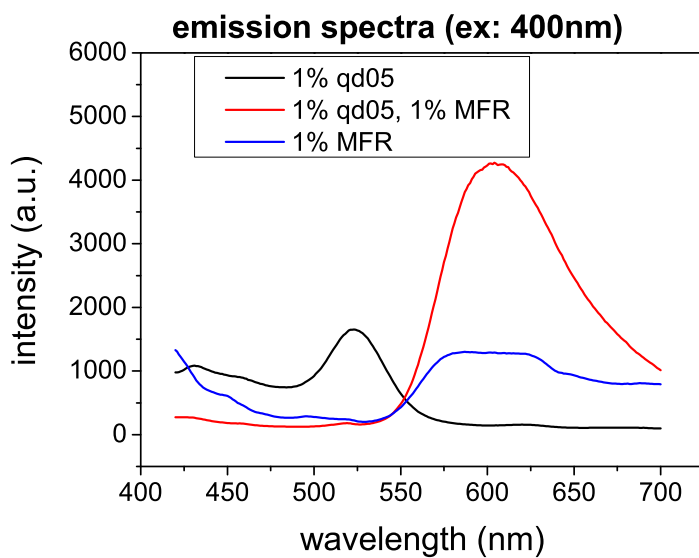


Figure 12.7: Emission of foils with qd05 (1%), MACROLEX Fluorescent Red G (MFR) (1%) and both (1% each).

13 Polymerization and characterization of the shell

In chapter 11 the production and functionalization of core particles was discussed. Here, the addition of a shell by polymerization is described. This shell also can be functionalized by co-polymerization of sensor dyes for example. Also the material can already exhibit special properties. The following pages will show that a shell does not hinder sensing abilities of the core and can also act as a sensor itself.

13.1 pNIPAAm - magnetic thermoresponsive oxygen sensors

In chapter 11 on page 47 two different oxygen sensors have already been characterized. They were core particles with integrated sensor dyes. A third batch was also co-precipitated with the oxygen indicator: Ir(Cs)₂(acac). Those particles (EIr) form the basis for oxygen sensitive core-shell particles (EIrP). In a radical chain reaction, *N*-isopropylacrylamide (NIPAAm) was polymerized using the EIr-core particles as reaction seeds. As cross-linker, *N,N'*-methylenebis(acrylamide) (BIS) was used. During polymerization, the particles grew from 121 to 217 nm hydrodynamic diameter. This means, a pNIPAAm shell of approximately 50 nm (at a temperature of 25°C) was built. pNIPAAm is known for its thermoresponsive behavior, as discussed in chapter 5 on page 24. Below the LCST the polymer is swollen just like a typical hydrogel. But above the LCST the structures collapse and the polymer pushes out the water. This results in a rather abrupt size change in the region of the LCST. To verify this characteristic of the particles, three consecutive measurements on the Zetasizer were performed. The temperature was raised in steps of 1°C. After an equilibration time of 25 min the sample was measured three times. The covered temperature range was 16 to 45°C. Figure 13.1 shows the results. As expected, the particles shrink when a temperature of 29°C is exceeded. At 38°C they have almost reached their final size in the collapsed condition. The LCST of the particles is at 34°C which is 2°C higher than the one of pNIPAAm in water.⁵⁰ As stated before, hydrophilic moieties can increase the LCST of the polymer. Here, BIS is believed to be responsible for the shift. Interestingly, the first run shows a higher starting size than the following ones. An explanation could be that the particles reversibly aggregated. During the phase transformation at the LCST this aggregation was eliminated. The run of the curve strengthens this theory. After the LCST, all three measurements reveal nearly the same sizes.

After proving the thermoresponsive properties of the synthesized particles, their ability for oxygen sensing was characterized. The corresponding Stern-Volmer plot can be seen in figure 13.2. Two measurements at 25°C and 40°C were carried out. The determined K_{SV} values are 0.0017 hPa⁻¹ for 25°C and 0.0026 hPa⁻¹ for 40°C. This experiment confirms the necessity of temperature-correction.

With these particles it was proven that the pNIPAAm shell does not disturb the sensing properties of the magnetic core. This clears the way for magnetic core-shell sensor particles

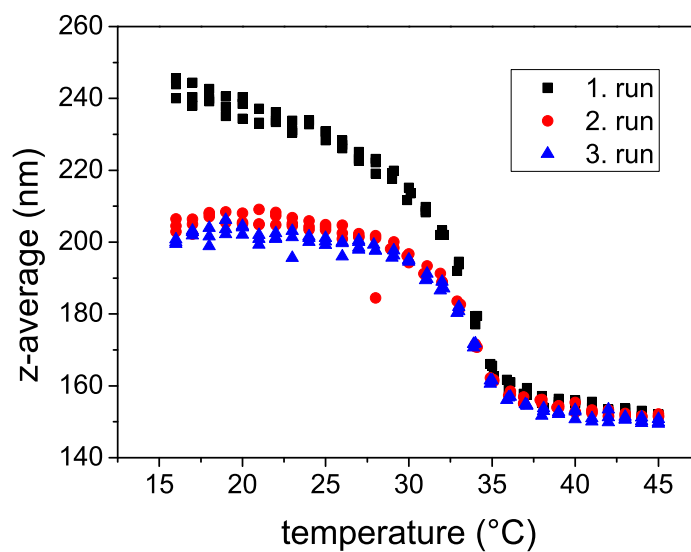


Figure 13.1: Dependence of z-average of the EIrP particles on the temperature. 3 runs on the Zetasizer were done.

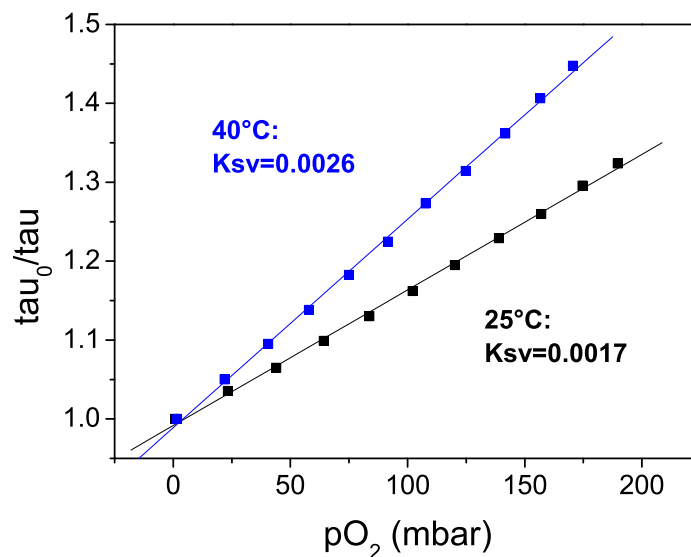


Figure 13.2: Stern-Volmer plot of the EIrP particles at 25°C ($K_{SV}=0.0017$) and 40°C ($K_{SV}=0.0026$).

with functionalization in the core as well as in the shell.

13.2 Acrylamide - magnetic pH sensor particles

Next to oxygen sensors, pH sensitive core-shell particles were produced. The knowledge of the pH of a system is one of the basic requirements in life science. The well-established pH electrode offers a very convenient and reliable system but still has some drawbacks. The physical dimension is too large for a multitude of applications and it is an invasive method. Magnetic optical sensor particles (MOSePs) can overcome these drawbacks. They form stable aqueous dispersions and measurement happens noninvasively. Furthermore, the particles of a hydrodynamic diameter of approximately 150 nm are small enough for applications in microfluidic systems. The magnetism of the particles permits separation of the particles by an external magnetic field. As the MOSePs can be placed directly in front of fiber optics with special separators,¹ the amount of MOSePs needed for measurement can be reduced significantly compared to dispersed systems. Also, the particles can be retained by a magnetic field in a region of interest, as it may be necessary in microfluidics, for example.

13.2.1 MOSePs for pH measurement

The here reported particles are based on a core-shell assembly. The core particles again are precipitated and allocate the magnetic properties. The matrix of the shell is poly(acrylamide) (pAAm), which is highly cross-linked with BIS to avoid extensive swelling of the particles in aqueous media. The measurement of pH is based on a ratiometric evaluation of the fluorescence of the indicator dye *N*-fluorescein-acrylamide (FLAC) and the rhodamine derivative ASRB (acryloylpiperazinyl sulforhodamine B) as reference dye, which is not affected by pH. By calculating the ratio of the emission intensities of those two dyes, the signal of the sensor becomes nearly independent of the particle concentration. Furthermore, sources of irritation, such as fluctuations of the excitation light or background luminescence, are eliminated. The sizes of the magnetic core particles (PH) were measured by dynamic light scattering. The hydrodynamic diameter of the core particles was 100 nm at a PDI value of 0.8. After polymerization of the acrylamide around the cores, the hydrodynamic diameter extended to 150 nm at PDIs of 0.5. Figure 13.3 shows a zero-loss TEM image of the core-shell particles (PHP). As the particles were dried in the course of sample preparation, the hydrogel shell shrank. As expected, it can not be seen on the image. During the polymerization, also the zeta-potential was measured and decreased from -25 to -4 mV. This proved that the acidic moieties of the core are shielded by the surrounding acryl amide matrix.

The luminescence of the particles depending on the pH and also the ionic strength was measured. The particles were dispersed in buffer solutions with ionic strengths of 15 to 500 mM and pH 3 to 12. The ratio of the luminescence intensities at 520 nm (emission maximum of FLAC) and 600 nm (emission maximum of the rhodamine derivative) was calculated. Plotting this data showed a dynamic range of the pH sensitive particles between pH 6 and 8 (figure 13.4). Furthermore, the pKa-values show only a minor dependency on the ionic strength of the solution (table 13.1 and figure 13.5). This is an already well-known and appreciated property of fluorescein. As the pKa values are at pH 7, application of the MOSePs for measurement in physiological conditions is ideal.

The response time of the pH-sensitive MOSePs was measured on a lock-in amplifier by changing the pH in steps of one unit from 6 to 8 and vice versa. This experiment in the

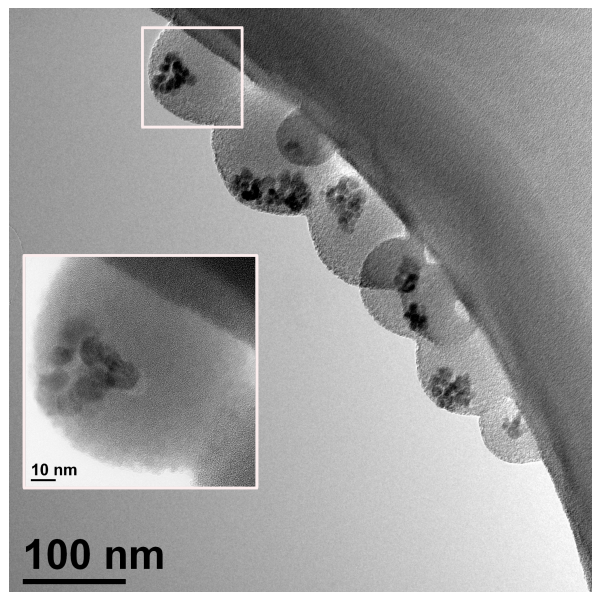


Figure 13.3: Zero-loss TEM image of the PHP particles.

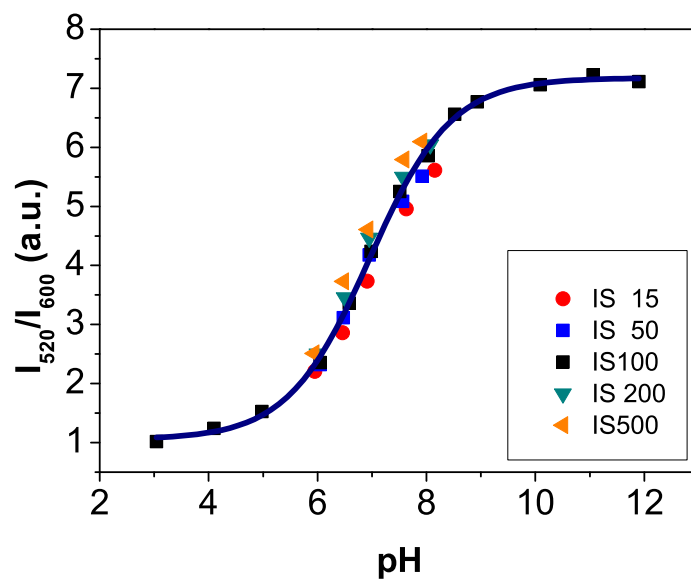
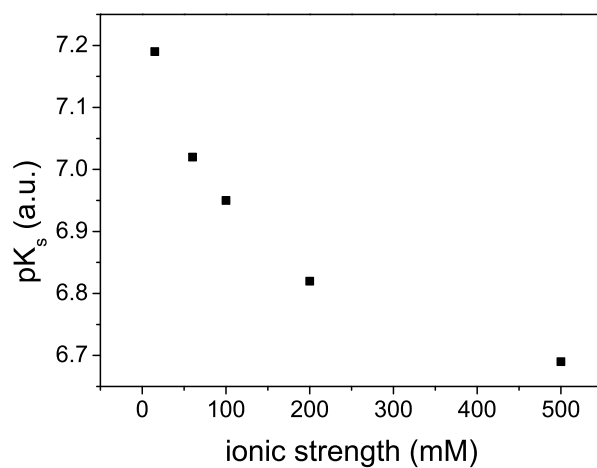


Figure 13.4: Relative fluorescence intensity of the PHP particles in dependency of the pH and ionic strength.

Table 13.1: pKa values of the PHP particles at varying ionic strengths.

Ionic strength (mM)	pKa values (a.u.)
15	7.19
50	7.02
100	6.95
200	6.82
500	6.69

**Figure 13.5:** Dependency of the pKa value on the ionic strength of the PHP particles.

dynamic range showed a reversible and stable signal response with an average value of t_{90} of only 3.2 seconds (figure 13.6).

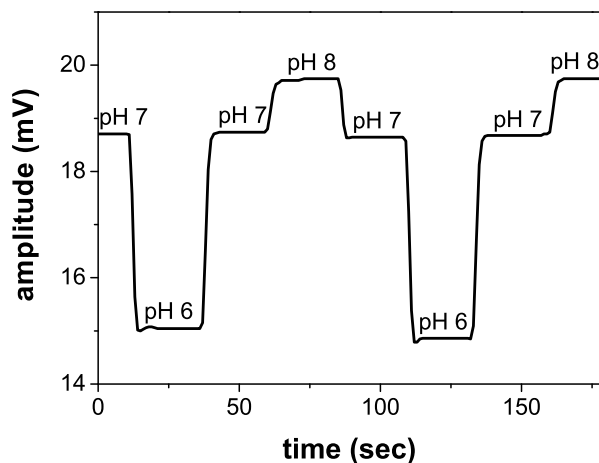


Figure 13.6: Signal reversibility of the pH sensitive MOSePs.

The here reported MOSePs are applicable for pH measurements in the range of pH 6 to 8. They are adequate for medical purposes, as the dynamic range covers physiological conditions. Due to their size of less than 200 nm, implementation in microfluidic systems for imaging purposes is possible. As they can be collected by an external magnetic field, a lower amount of particles is needed compared to dispersions. Furthermore, the signal is independent on particle concentration because of the ratiometric measurement.

Measurement of pH in aqueous media in the range of pH 6 to 8 is reversibly possible. As the particles can be collected in front of fiber optics with a special separator, signal enhancement is easily achieved, resulting in a low concentration of MOSePs needed for investigations. By using MOSePs pH measurement is possible by a noninvasive technique which requires no further preparation steps such as the application of a sensor foil into a reaction vessel.

13.3 pNIPAAm - magnetic fructose sensor particles

A previous work of our group was the development of a glucose and fructose sensor⁴⁶ based on FRET. Here, pNIPAAm particles were produced with covalently bond 3-acrylamidophenylboronic acid and the two fluorophores FLAC (*N*-fluorescein-acrylamide) and ASRB (acryloylpiperazinyl sulforhodamine B). By excitation of FLAC and with a distance between FLAC and ASRB lower than approximately 10 nm, an energy transfer occurs and the emitted light originates mainly of the ASRB molecules. The boronic acid attracts sugar molecules leading to a swelling of the pNIPAAm particles. Thereby the distance between the two dyes becomes larger, thus preventing the FRET mechanism. The emitted light now is produced by FLAC. By recording the ratio of the intensities of both emission maxima, the concentration of glucose and fructose, respectively, can be measured via the change of particle size.

Knowing that, it was obvious to try to combine this already existing sensor principle with

the core-shell approach of my thesis. With a magnetic core and a sugar responsive shell, magnetic collection of the sensors would be possible.

13.3.1 Core-shell particles with a pNIPAAm/FLAC shell

In the beginning, magnetic core particles (SU) were covered with a pNIPAAm shell which was cross-linked with BIS and co-polymerized with FLAC (SUP1). The fluorescence intensity of FLAC showed a high dependency on temperature. In order to understand this phenomenon, a suspension of the particles in deionized water and in phosphate buffer (pH 8, 100 mM) was excited at 490 nm and the emission of FLAC was recorded (figures 13.7 and 13.8). Furthermore, the hydrodynamic diameter of the particles was determined (figure 13.9). In water, the intensity signal changed by 80 % in the investigated temperature range. In contrast, the signal change in buffer was only 35 %. This observation leads to the assumption that the intensity change is mainly induced by the change of the pH value of water of different temperatures. Another possibility would be that the changing polarity of the pNIPAAm matrix, caused by the temperature change, effects the luminescence of the FLAC molecules. As can be seen in figure 13.9, the LCST of the particles is approximately at 35°C. In figure 13.10 the maximum intensity of both suspensions is plotted against temperature. It is evident that the biggest change of luminescence signal is between 30 and 32°C. This does not correlate with the LCST of the polymer. Therefore, the temperature dependent pH of water seems to be the originator of the difference of the signal-intensities in buffer and water.

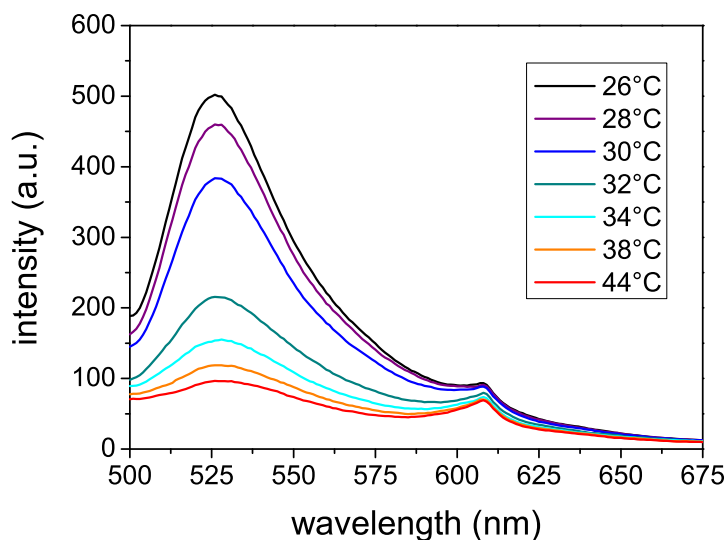


Figure 13.7: Emission spectrum of SUP1 particles in water at changing temperatures. The excitation wavelength was 490 nm.

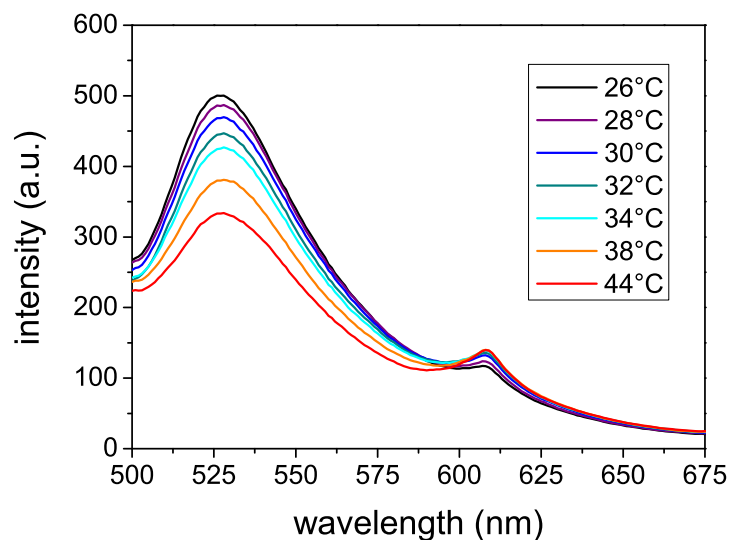


Figure 13.8: Emission spectrum of SUP1 particles PBS (100 mM, pH 8) at changing temperatures. The excitation wavelength was 490 nm.

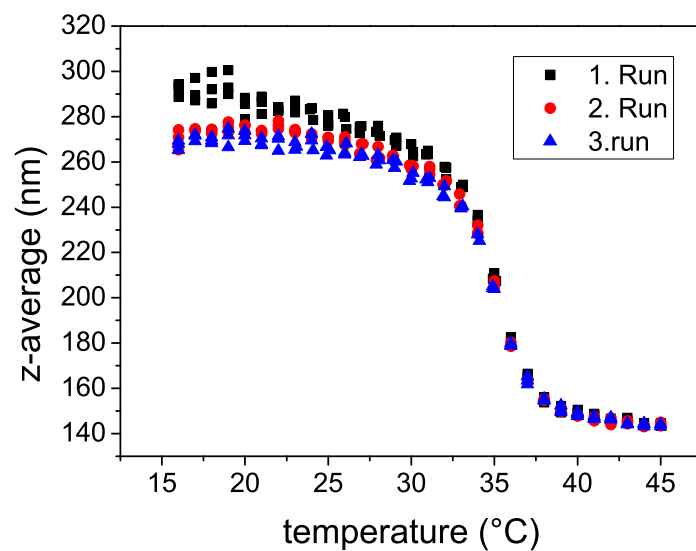


Figure 13.9: Thermoresponsive behavior of the SUP1 particles. 3 runs on the Zetasizer were carried out.

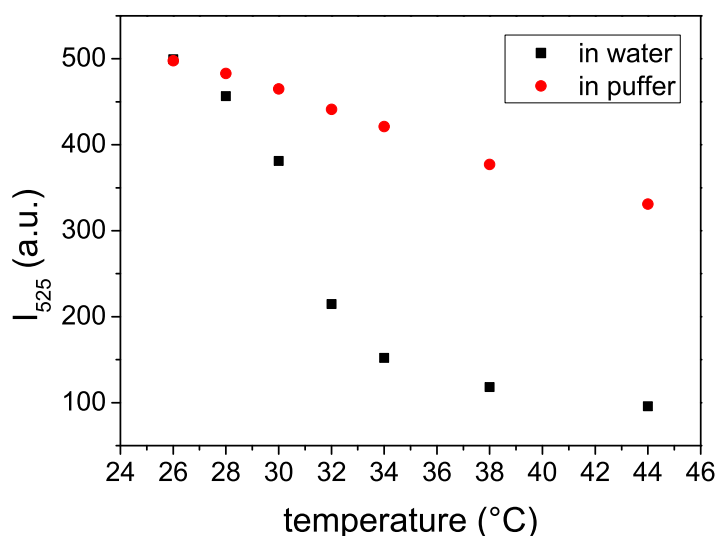


Figure 13.10: Fluorescence intensity of the SUP1 particles in water and buffer (pH 8, 100 mM), respectively, at varying temperatures.

13.3.2 Fructose/Glucose sensor particles

The particles designed for sugar analysis were again produced by co-polymerization of the shell around precipitated magnetic core particles. Here, the shell consists of a relatively complex matrix. Next to pNIPAAm, which is cross-linked with BIS, also the two indicator dyes FLAC (as acceptor) and ASRB (as donor) as well as (4-allylaminocarbonylphenyl)boronic acid (BA) as the fructose/glucose receptor are integrated (SUP2). The change of the relative fluorescence of the two indicator dyes (I_{525}/I_{595}) and of the hydrodynamic diameter after addition of a fructose and glucose solution were measured. After addition, the sample had a sugar concentration of 2.48 mg mL^{-1} or 13.7 mM . For comparison reasons, also the addition of a same volume of buffer solution was monitored. In figure 13.11 the increase of the signal after addition of fructose can be seen. For the glucose as well as the buffer solution no response was noticed. It is known that the boronic acid has a higher affinity for fructose than for glucose. In order to obtain a signal also for glucose, maybe a concentration of approximately 200 mM would have been necessary. The change of the hydrodynamic diameter (figure 13.12) corresponds to the fluorescence data. Here again, only addition of fructose resulted in a swelling of the particles. Figures 13.13 and 13.14 compare the luminescence ratio to the size change after addition of fructose and glucose, respectively. In the case of fructose it can be seen that the volume change happens very fast (addition of the sugar at 0 min). Due to the measurement method it was not possible to obtain more values for the hydrodynamic diameter for the interesting region of 0 min to 5 min. Nevertheless, an immediate response takes place.

This experiment verifies that the concept of a sugar sensor based on FRET is applicable on the core-shell design. For glucose measurements higher concentrations of sugar would be needed. Furthermore, a constant temperature during measurement is necessary, as the

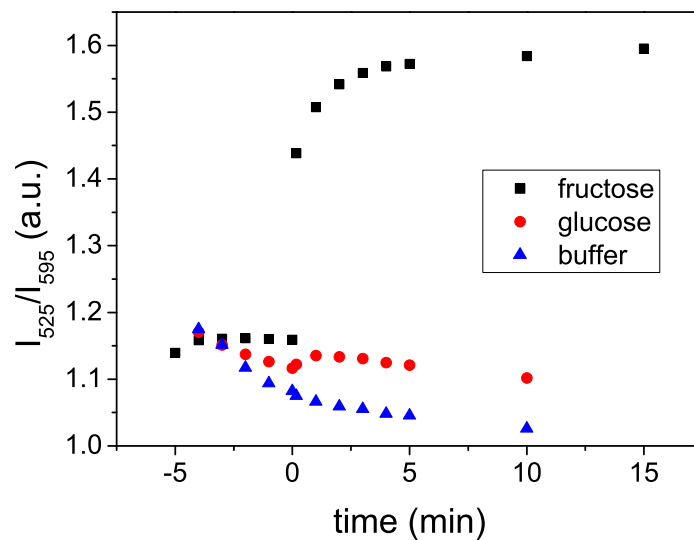


Figure 13.11: Relative fluorescence intensity of the SUP2 particles in dependence of the presence of fructose and glucose or only buffer. Addition of sugars/buffer at 0 min.

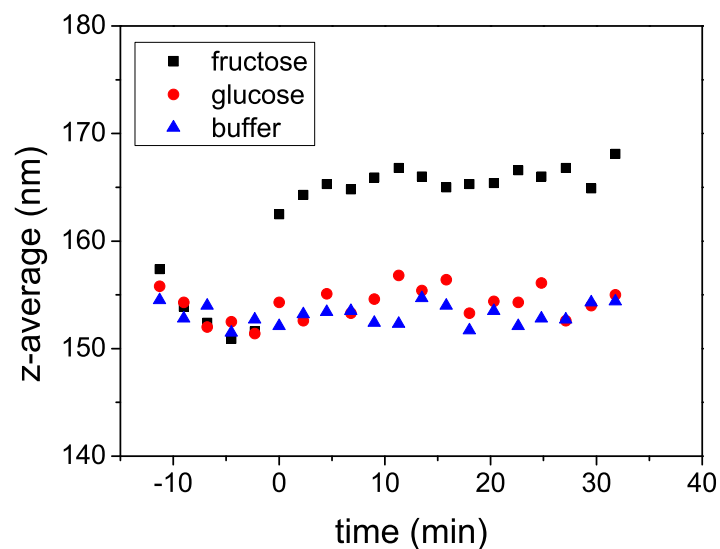


Figure 13.12: SUP2 particle sizes after addition of fructose, glucose and buffer. Addition of sugars/buffer at 0 min.

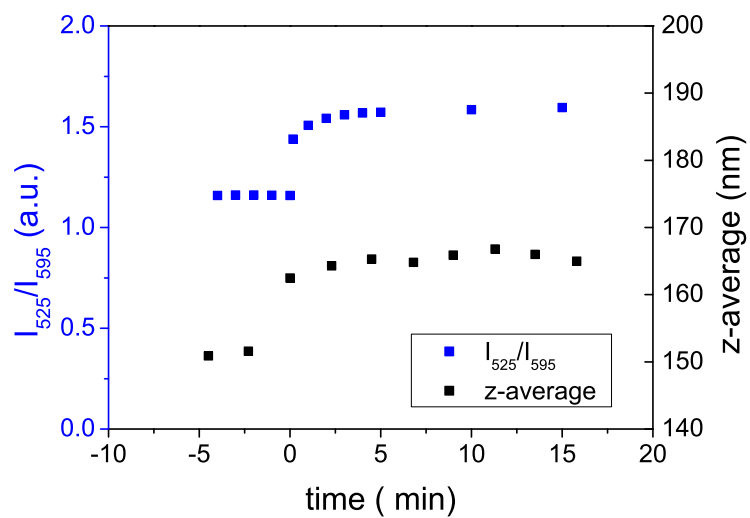


Figure 13.13: Comparison of the relative fluorescence and z-average (SUP2). Addition of fructose at 0 min.

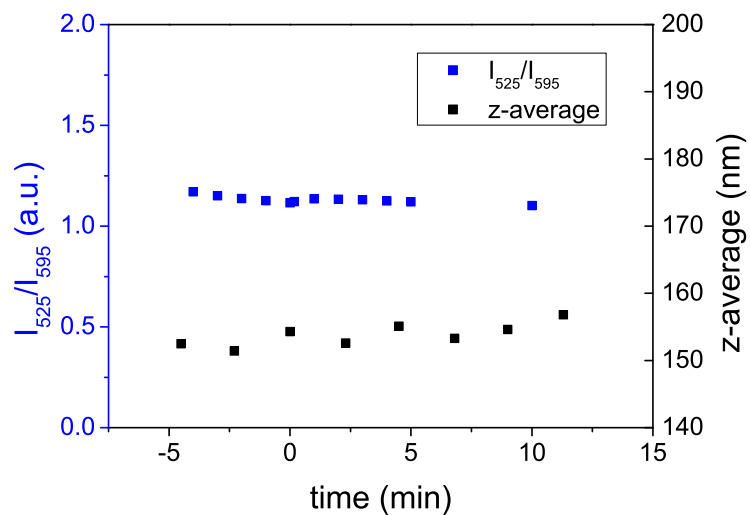


Figure 13.14: Comparison of the relative fluorescence and z-average (SUP2). Addition of glucose at 0 min.

luminescence of fluorescein in this matrix is apparently temperature dependent.

13.4 pNIPAAm - magnetic thermoresponsive particles for drug delivery?

With its unique thermoresponsive properties, pNIPAAm has attracted interest in the field of drug delivery systems. Due to the phase transformation of this polymer at the LCST a controllable release of a loaded active pharmaceutical ingredient should be possible. Some positive results using micelles partially made of pNIPAAm are already published. It was possible to load the particles with a model drug and release it in different velocities, depending on the temperature. Knowing that, I was curious if the concept of the core-shell particles is also adaptable for drug delivery.

13.4.1 Synthesis of the core-shell particles

At first, core-shell particles with a pNIPAAm shell, cross-linked with BIS, were synthesized. The particles used for the drug loading experiments are labeled as DLP1 to DLP6, with DD particles as cores. DLP1 to DLP3 have a different BIS content, resulting in an unequal degree of cross-linking. During experiments a polymerization without SDS was carried out successfully. This is a very desirable situation, as the cleaning is much easier and less time-consuming without an emulsifier. From that moment on, all polymerizations were carried out without SDS. It seems that SDS deactivates PPS to some extent, as the necessary amount of it shrank to a quarter. For DLP4 to DLP6 higher concentrations of BIS (9 and 12 mol%) were used. The particles were washed three times prior to the drug loading experiments.

Table 13.2: Relevant parameters for the synthesis of DLP1 to DLP6.

Particles	SDS (mM)	BIS (mol%)	PPS (mg)	Temperature (°C)
DLP1	1.25	2.5	12	75
DLP2	1.25	5.2	12	75
DLP3	1.25	9.0	12	75
DLP4	0	9.0	6	70
DLP5	0	9.0	3	70
DLP6	0	12.0	3	70

13.4.2 Drug loading experiments

DLP1-3 In this first drug loading experiment particles with a varying degree of cross-linker were used. They were dissolved in an aqueous Brilliant Blue FCF (a blue colorant for foods) solution and incubated for 24 hours. DLP1a to DLP3a were kept at room temperature while DLP1b to DLP3b were kept in a water bath at 40°C. After incubation, they were magnetically collected and the supernatant was drawn off and replaced with deionized water (of either room temperature or 40°C, respectively). This procedure had to be repeated twice, as the loading medium could not be removed in a sufficient quantity in the first time. For the DLP1a

to DLP3a particles, absorption of the supernatant was measured. Then the particles were heated in a water bath for one hour. Now again, absorption was measured. For the DLP1b to DLP3b particles, absorption first was determined at 40°C and then again after cooling the particles down. In no case, a release of the colorant could be observed. As the absorption of the loading medium was not recorded before and after incubation, it was not possible to determine if loading was successful. Therefore, it could be possible that the colorant either was not loaded at all or was loaded onto the particles but did not diffuse into the solution. Furthermore, the separation of the particles after incubation took several hours. Potentially loaded colorant molecules might be released by diffusion during the washing steps of separation.

DLP4 In this experiment the particles were lyophilized prior to the loading step. It was thought that loading would be more efficient if the particles absorb the surrounding medium like a sponge than in the case when they are already swollen. The lyophilized particles were dissolved in a PBS with Brilliant Blue FCF and incubated for 24 hours at 27°C. After magnetic collection of the particles, the supernatant was drawn off and the particles dispersed in PBS. Absorption measurements of the loading medium before and after incubation showed a loaded amount of 2 wt%. For release measurement, the particles were heated up to 45°C in the water bath and after equilibration and collection of the particles, absorption was measured again. Unfortunately, no release could be determined. As the particles could not be separated completely they were an interference factor for absorption measurement. It could be possible that the dye loaded on the particles was measured and not the dye in solution.

DLP5 The basic set up of this experiment was the same as in DLP4 but the particles were separated by centrifugation at 4,000 rpm for 30 min. But here again, the particles were not separated completely. Also, no drug release was observed, even though a loaded amount of 1.2 wt%, based on absorption measurements of the loading medium before and after incubation, was calculated.

DLP6 This experiment was the last attempt for drug loading. Here the basic set up was similar to DLP5, but now ampicillin was used as model drug. Separation was accomplished by centrifugation on an ultracentrifuge at 40,000 rpm for 30 min. In this case, separation was successful, but no released ampicillin could be detected by absorbance measurements.

To sum up, it can be said that the complexity of drug delivering particles was underestimated. There are a lot of factors contributing to loading and release procedures. In order to achieve a functioning and reliable system a lot of work has to be done. The produced particles appeared to offer too little possibilities to hold drug molecules. Maybe another layer between the core particles and pNIPAAm should be attached. This could provide the required storage capacities, while the surrounding pNIPAAm acts as a gate. Possible materials for this storage layer should exhibit a mesoporous structure. As a positive result of the drug delivery experiments the successful polymerization without an emulsifier can be mentioned. Washing steps become less time-consuming and more effective.

Part V

Conclusions and outlook

14 Core particles

14.1 Precipitation

The precipitation parameters influencing the core particle diameters were examined. Here, some important dependencies appeared. As a parameter with high impact on the resulting core size, the molecular weight as well as the concentration of the polymer in the cocktail were affirmed. A positive correlation occurs: the higher the molecular weight or concentration of the polymer used was, the bigger were the resulting particles. By changing this parameter, core particles with hydrodynamic diameters from 80 to 190 nm could be produced. Another significant influence has the concentration of magnetite in the cocktail. Apparently it acts as seed for the precipitating particles. As a result of this, the obtained particles become smaller with a higher concentration of magnetite, as more seeds are available for the same amount of polymer. By variation of the magnetite content a difference in size of 60 nm could be achieved. Changing the precipitation direction from CiP (cocktail into precipitant) to PiC (vice versa), the resulting particles are larger. Their hydrodynamic diameter is approximately 20 nm higher. As the dilution happens more slowly in this direction, consequently more time is available for the particles to form. Therefore, a favoured lower surface/volume ratio can be obtained. Change of the flow rate of injection affects the resulting particles in the range of 10 nm to 25 nm, while the vortex speed has no impact on it at all.

By varying the precipitation parameters a desired particle size can be adjusted. The possible range of the hydrodynamic diameter of produced particles is between 80 to 190 nm.

14.2 Functionalization

Next to the functionalization with magnetite, incorporation of indicator dyes was also possible. Three different oxygen sensitive luminescent dyes were integrated:

- Ir(Cs)₂(acac),
- PtTPTBPF and
- PdTPTBPF.

Particles equipped with Ir(Cs)₂(acac) or PtTPTBPF can detect oxygen in the range of 0 - 100 % airsaturation, whereas PdTPTBPF particles can act as trace oxygen sensors. Their range of application is between 0% and 5 % airsaturation. But not only the core particles can be used as oxygen sensors. Also the addition of a shell is possible without prohibiting the sensing properties. As a further step, additional functionalities could be applied in the shell.

15 QDs

The production of QDs was very successful. It was possible to produce QDs with a desired emission maximum in the range of 490 nm to 585 nm. This was possible by varying the reaction time. The longer the reaction lasted, the more time was available to grow for the QDs and, consequently, the longer was the emission wavelength. A comparison with commercially available QDs showed no significant difference in optical properties. The quantum yield of the synthesized QDs was only about one third lower. Against our expectation, the quantum yields of QDs are in the range of 10 %. Compared to the luminescent dyes used in our group, this is a very low value. Integration of QDs in foils for light harvesting purposes worked only once, while the integration in particles by co-precipitation did not work at all. Obviously, there are still a lot of parameters to control for working with QDs. Hard work will have to be done in order to achieve the incorporation of QDs for uses in energy transfer systems. But as the optical properties of QDs are not even near to the expected, further investigation was considered to be redundant.

16 Core-shell particles

The application of three different sensor types on the core-shell particles was possible. The core as well as the shell can be functionalized in order to achieve sensing properties.

16.1 Oxygen sensors

For oxygen sensors, the indicator dye was co-precipitated into the core. The attachment of a shell does not affect the sensing properties. An additional functionalization of the shell is also possible. This might enable simultaneous detection of two analytes, for example.

16.2 pH sensors

By equipping the shell with a pH sensitive dye and a reference dye, pH sensitive particles were created. The measurement is based on a ratiometric readout of the two dyes. This makes the signal almost independent of the particle concentration and compensates perturbations such as fluctuations of the emission light or background luminescence. With the synthesized particles it is possible to determine pH in the physiological range (pH 6 - 8). Also, the signal has only a very low cross-sensitivity to the ionic strength of the medium. With a short response time of 3.2 seconds in average, it is adequate for most applications. Due to the magnetic properties, the particles can be collected in front of fiber optics, thus reducing the needed amount of particles for investigation. Furthermore, due to their small dimensions of less than 200 nm the pH sensitive MOSePs might be applicable for microfluidics and imaging.

16.3 Fructose sensors

Also the adaption of fructose sensors based on FRET was possible. It was observed that the measurements have to be carried out in buffered and thermostatted solutions. Otherwise the pH of an aqueous solution would be temperature dependent and this would lead to a signal change of the donor dye. By recording the ratiometric signal of donor and acceptor dye, it was possible to detect fructose. Also, a swelling of the particles correlated to the signal change was observed. Unfortunately, glucose could not be detected. But it is known that boronic acid has a higher affinity to fructose than to glucose. As a result, detection limits for glucose are much higher than for fructose.

16.4 Drug delivery

The idea of loading the shell with active pharmaceutical ingredients and releasing them by a change of temperature was much more difficult to realize than assumed. The complexity of the system was underestimated. Furthermore, the application of an additional layer which

can act as storage for the molecules might be necessary. The pNIPAAm shell could act as a temperature controllable gate in such a system. But as a positive result yielding from these experiments, the polymerization of the shell without emulsifier can be stated. This is a big advantage, as washing steps after synthesis can be minimized.

List of Figures

1.1	Set up of a typical sensor	8
1.2	Components of an optical sensor	9
2.1	Possible relaxation pathways of an excited molecule	11
2.2	The Perrin-Jablonski diagram	13
2.3	Forms of fluorescein in aqueous solution	17
3.1	Diamagnetic and paramagnetic matter	20
5.1	Chain polymerization scheme	23
5.2	The three stages of a radical chain polymerization	24
5.3	Structures of FLAC and ASRB	25
6.1	The hydrodynamic diameter of a particle	28
11.1	Dependency of z-average on polymer type and concentration	44
11.2	Influence of the precipitation direction on the particle size	45
11.3	Particle sizes at different vortex speeds	45
11.4	The effect of cocktail injection velocity on z-average	46
11.5	The influence of magnetite concentration on the hydrodynamic diameter	47
11.6	Stern-Volmer plot of PtTPTBPF	48
11.7	Stern-Volmer plot of PdTPTBPF	49
11.8	Structures of Ir(Cs) ₂ (acac), PtTPTBPF and PdTPTBPF	49
12.1	The dependency of the emission of the QDs on the reaction time	52
12.2	Normalized absorption, excitation and emission spectra of qd01	53
12.3	Absorption spectra of EviDot and qd03	55
12.4	Emission spectra of EviDot and qd03	55
12.5	Excitation spectra of EviDot and qd03	56
12.6	Absorption of foils	57
12.7	Emission of foils	57
13.1	EIRP particles - dependence of z-average on the temperature	60
13.2	Stern-Volmer plot of the EIRP particles	60
13.3	Zero-loss TEM image of the PHP particles	62
13.4	pH curve of the PHP particles	62
13.5	Dependency of the pKa value on the ionic strength	63
13.6	Signal reversibility of the PHP particles	64
13.7	Emission spectrum of SUP1 particles in water	65
13.8	Emission spectrum of SUP1 particles in PBS	66
13.9	Thermoresponsive behavior of the SUP1 particles	66

List of Figures

13.10	Fluorescence signal of the SUP1 particles at varying temperatures	67
13.11	Relative fluorescence intensity of the SUP2 particles in presence of sugars . . .	68
13.12	SUP2 particle sizes in presence of sugars	68
13.13	Fluorescence and z-average of SUP2 with fructose	69
13.14	Fluorescence and z-average of SUP2 with glucose	69

List of Tables

2.1	Characteristic decay times of photophysical processes.	14
3.1	The three types of magnetism	19
7.1	Devices used for this thesis	31
7.2	Chemicals used for this thesis	32
8.1	Instructions for the precipitation of the core particles, part 1	34
8.2	Instructions for the precipitation of the core particles, part 2	35
8.3	Properties of EF-80 and PSMA93	36
8.4	Settings of the lock-in amplifier	36
9.1	Utilized quantities of reagents for shell polymerization	38
11.1	Characteristics of EF-80 and PSMA93	43
11.2	Photo-physical properties of the used indicators	48
12.1	Em_{max} , Abs_{max} and ϕ of some synthesized QDs	53
12.2	Concentrations of the QD solutions	54
13.1	pKa values of the PHP particles at varying ionic strengths	63
13.2	Relevant parameters for the synthesis of DLP1 to DLP6	70

Bibliography

- [1] G. Mistlberger, P. Chojnacki, and I. Klimant. Magnetic sensor particles: an optimized magnetic separator with an optical window. *J. Phys. D: Appl. Phys.*, 41(8), 2008.
- [2] G. Mistlberger, S. M. Borisov, and I. Klimant. Enhancing performance in optical sensing with magnetic nanoparticles. *Sens. Actuators, B*, 139(1, Sp. Iss. SI):174–180, 2009.
- [3] A. Hulanicki, S. Glab, and F. Ingman. Chemical sensors definitions and classification. *Pure Appl. Chem.*, 63(9):1247–1250, 1991.
- [4] J. Janata and A. Bezech. Chemical sensors. *Anal. Chem.*, 60(12):R62–R74, 1988.
- [5] O. Wolfbeis. Chemical sensors - survey and trends. *Fres. J. Anal. Chem.*, 337(5):522–527, 1990.
- [6] P. Gründler. *Chemische Sensoren: Eine Einführung für Naturwissenschaftler und Ingenieure*. Springer, Berlin, 1 edition, March 2004. ISBN 3540209840.
- [7] S. M. Borisov and I. Klimant. Optical nanosensors - smart tools in bioanalytics. *Analyst (Cambridge, U. K.)*, 133(10):1302–1307, 2008.
- [8] J. Aylott. Optical nanosensors - an enabling technology for intracellular measurements. *Analyst (Cambridge, U. K.)*, 128(4):309–312, 2003.
- [9] H. Clark, S. Barker, M. Brasuel, M. Miller, E. Monson, S. Parus, Z. Shi, A. Song, B. Thorsrud, R. Kopelman, A. Ade, W. Meixner, B. Athey, M. Hoyer, D. Hill, R. Lightle, and M. Philbert. Subcellular optochemical nanobiosensors: probes encapsulated by biologically localised embedding (pebbles). *Sens. Actuators, B*, 51(1-3):12–16, 1998.
- [10] P. Chojnacki, G. Mistlberger, and I. Klimant. Separable magnetic sensors for the optical determination of oxygen. *Angew. Chem., Int. Ed.*, 46(46):8850–8853, 2007.
- [11] L. J. Lauhon, M. S. Gudiksen, D. Wang, and C. M. Lieber. Epitaxial core-shell and core-multishell nanowire heterostructures. *Nature (London, United Kingdom)*, 420(6911):57–61, 2002.
- [12] Y. Deng, W. Yang, C. Wang, and S. Fu. A novel approach for preparation of thermoresponsive polymer magnetic microspheres with core-shell structure. *Adv. Mater.*, 15(20):1729–1732, 2003.
- [13] Y. Wang, S. Gao, W. Ye, H. S. Yoon, and Y. Yang. Co-delivery of drugs and DNA from cationic core-shell nanoparticles self-assembled from a biodegradable copolymer. *Nat. Mater.*, 5(10):791–796, 2006.

- [14] A. J. Patil, E. Muthusamy, and S. Mann. Synthesis and self-assembly of organo-clay-wrapped biomolecules. *Angew. Chem., Int. Ed.*, 43(37):4928–4933, S4928/1–S4928/12, 2004.
- [15] E. M. Dibbern, F. J. Toublan, and K. S. Suslick. Formation and characterization of polyglutamate Core-Shell microspheres. *J. Am. Chem. Soc.*, 128(20):6540–6541, 2006.
- [16] A. Burns, P. Sengupta, T. Zedayko, B. Baird, and U. Wiesner. Core/shell fluorescent silica nanoparticles for chemical sensing: towards single-particle laboratories. *Small*, 2(6):723–726, 2006.
- [17] Y. Mei, Y. Lu, F. Polzer, M. Ballauff, and M. Drechsler. Catalytic activity of palladium nanoparticles encapsulated in spherical polyelectrolyte brushes and core-shell microgels. *Chem. Mater.*, 19(5):1062–1069, 2007.
- [18] C. Liu, J. Guo, W. Yang, J. Hu, C. Wang, and S. Fu. Magnetic mesoporous silica microspheres with thermo-sensitive polymer shell for controlled drug release. *J. Mater. Chem.*, 19:4764–4770, 2009.
- [19] S. Q. Liu, Y. W. Tong, and Y.-Y. Yang. Incorporation and in vitro release of doxorubicin in thermally sensitive micelles made from poly(n-isopropylacrylamide-co-n, n-dimethylacrylamide)-b-poly(d, l-lactide-co-glycolide) with varying compositions. *Biomaterials*, 26:5064–5074, 2005.
- [20] C. Yan, A. Elaissari, and C. Pichot. Loading and release studies of proteins using poly(n-isopropylacrylamide) based nanogels. *J. Biomed. Nanotechnol.*, 2:208–216, 2006.
- [21] B. Valeur. *Molecular Fluorescence - Principles and Applications*. Wiley-VCH, Weinheim, 1 edition, 2002. ISBN 3-527-29919-X.
- [22] E. R. Carraway, J. N. Demas, and B. A. DeGraff. Luminescence quenching mechanism for microheterogeneous systems. *Anal. Chem.*, 63(4):332–6, 1991.
- [23] I. Klimant, F. Ruckruh, G. Liebsch, A. Stangelmayer, and O. S. Wolfbeis. Fast response oxygen micro-optodes based on novel soluble ormosil glasses. *Microchimica Acta*, 131(1-2):35–46, 1999.
- [24] E. Riedel. *Anorganische Chemie*. de Gruyter, 5 edition, 2002. ISBN 3-11-017439-1.
- [25] A. M. Smith and S. Nie. Semiconductor nanocrystals: Structure, properties, and band gap engineering. *Acc. Chem. Res.*, 43(2):190–200, 2010.
- [26] M. F. Frasco and N. Chaniotakis. Semiconductor quantum dots in chemical sensors and biosensors. *Sensors*, 9(9):7266–7286, 2009.
- [27] W. C. Chan, D. J. Maxwell, X. Gao, R. E. Bailey, M. Han, and S. Nie. Luminescent quantum dots for multiplexed biological detection and imaging. *Curr. Opin. Biotechnol.*, 13(1):40–46, 2002.
- [28] E. Scher, L. Manna, and A. Alivisatos. Shape control and applications of nanocrystals. *Philos. Trans. R. Soc. London, Ser. A*, 361(1803):241–255, 2003.

-
- [29] B. Dabbousi, J. RodriguezViejo, F. Mikulec, J. Heine, H. Mattoussi, R. Ober, K. Jensen, and M. Bawendi. (cdse)zns core-shell quantum dots: Synthesis and characterization of a size series of highly luminescent nanocrystallites. *J. Phys. Chem. B*, 101(46):9463–9475, 1997.
- [30] C. Xu and E. Bakker. Multicolor quantum dot encoding for polymeric particle-based optical ion sensors. *Anal. Chem. (Washington, DC, U. S.)*, 79:3716–3723, 2007.
- [31] M. Koneswaran and R. Narayanaswamy. Mercaptoacetic acid capped cds quantum dots as fluorescence single shot probe for mercury(ii). *Sens. Actuators, B*, 139(1, Sp. Iss. SI): 91–96, 2009.
- [32] W. R. Algar and U. J. Krull. Quantum dots as donors in fluorescence resonance energy transfer for the bioanalysis of nucleic acids, proteins, and other biological molecules. *Anal. Bioanal. Chem.*, 391:1609–1618, 2008.
- [33] S.-H. Choi, H. Song, I. K. Park, J.-H. Yum, S.-S. Kim, S. Lee, and Y.-E. Sung. Synthesis of size-controlled cdse quantum dots and characterization of cdse-conjugated polymer blends for hybrid solar cells. *Journal of Photochemistry and Photobiology A: Chemistry*, 179(1-2):135 – 141, 2006.
- [34] P. Xue. Quantum computing with semiconductor double-dot molecules on a chip. *Quantum Physics*, pages 1–5, arXiv:0908.3719v1 [quant-ph], 2009.
- [35] A. Clapp, I. Medintz, and H. Mattoussi. Forster resonance energy transfer investigations using quantum-dot fluorophores. *ChemPhysChem*, 7(1):47–57, 2006.
- [36] A. M. Coto-Garcia, M. T. Fernandez-Arguelles, J. M. Costa-Fernandez, and A. Sanz-Medel. Entrapment of quantum dots in sol-gel matrices to develop sensing material based on fluorescence resonance energy transfer. *Chem. Commun. (Cambridge, U. K.)*, pages 5454–5456, 2009.
- [37] G. Odian. *Principles of Polymerization*. Wiley-Interscience, 4 edition, 2004. ISBN 0-471-27400-3.
- [38] A. Jenkins, P. Kratochvil, R. Stepto, and U. Suter. Glossary of basic terms in polymer science. *Pure Appl. Chem.*, 68(12):2287–2311, 1996.
- [39] A. Hoffman. Hydrogels for biomedical applications. *Adv. Drug Delivery Rev.*, 54(1):3–12, 2002.
- [40] H. Yang and W. J. Kao. Thermoresponsive gelatin/monomethoxy poly(ethylene glycol)-poly(d,l-lactide) hydrogels: Formulation, characterization, and antibacterial drug delivery. *Pharm. Res.*, 23:205–214, 2006.
- [41] H. H. Sokker, A. M. Abdel Ghaffar, Y. H. Gad, and A. S. Aly. Synthesis and characterization of hydrogels based on grafted chitosan for the controlled drug release. *Carbohydr. Polym.*, 75:222–229, 2009.
- [42] B. Jeong and A. Gutowska. Lessons from nature: stimuli-responsive polymers and their biomedical applications. *Trends Biotechnol.*, 20(7):305–311, 2002.

- [43] J. L. Zhang, R. S. Srivastava, and R. D. K. Misra. Core-shell magnetite nanoparticles surface encapsulated with smart stimuli-responsive polymer: Synthesis, characterization, and test of viable drug-targeting delivery system. *Langmuir*, 23:6342–6351, 2007.
- [44] Y. Zhu, S. Kaskel, T. Ikoma, and N. Hanagata. Magnetic sba-15/poly(n-isopropylacrylamide) composite: Preparation, characterization and temperature-responsive drug release property. *Microporous Mesoporous Mater.*, 123:107–112, 2009.
- [45] <http://www.malvern.com>, March 2010.
- [46] G. Zenkl, T. Mayr, and I. Klimant. Sugar-responsive fluorescent nanospheres. *Macromol. Biosci.*, 8:146–152, 2008.
- [47] S. M. Borisov and I. Klimant. Ultrabright oxygen optodes based on cyclometalated iridium(III) coumarin complexes. *Anal. Chem. (Washington, DC, U. S.)*, 79:7501–7509, 2007.
- [48] S. M. Borisov, G. Nuss, W. Haas, R. Saf, M. Schmuck, and I. Klimant. New NIR-emitting complexes of platinum(II) and palladium(II) with fluorinated benzoporphyrins. *Journal of Photochemistry and Photobiology A: Chemistry*, 201(2-3):128–135, 2009.
- [49] E. M. Boatman, G. C. Lisensky, and K. J. Nordell. A safer, easier, faster synthesis for CdSe quantum dot nanocrystals. *J. Chem. Educ.*, 82:1697–1699, 2005.
- [50] X. Xin-Cai, C. Liang-Yin, C. Wen-Mei, W. Shu, and X. Rui. Preparation of submicrometer-sized monodispersed thermoresponsive core-shell hydrogel microspheres. *Langmuir*, 20:5247–53.